

A seasonal model of the Mediterranean Sea general circulation

Vassil Roussenov,¹ Emil Stanev,¹ Vincenzo Artale,² and Nadia Pinardi

Istituto per lo Studio delle Metodologie Geofisiche Ambientali, Consiglio Nazionale delle Ricerche
Modena, Italy

Abstract. This paper describes the seasonal characteristics of the Mediterranean Sea general circulation as simulated by a primitive equation general circulation model. The forcing is composed of climatological monthly mean atmospheric parameters, which are used to compute the heat and momentum budgets at the air-sea interface of the model. This allows heat fluxes to be determined by a realistic air-sea interaction physics. The Strait of Gibraltar is open, and the model resolution is $\frac{1}{4} \times \frac{1}{4}$ in the horizontal and 19 levels in the vertical. The results show the large seasonal cycle of the circulation and its transient characteristics. The heat budget at the surface is characterized by lateral boundary intensifications occurring in downwelling and upwelling areas of the basin. The general circulation is composed of subbasin gyres, and cyclonic motion dominates the northern and anticyclonic motion the southern part of the basin. The Atlantic stream which enters from Gibraltar and assumes the form of different boundary current subsystems is a coherent structure at the surface. At depth it appears as current segments and jets around a vigorous gyre system. The seasonal variability is manifested not only by a change in amplitude and location of the gyres but also by the appearance of seasonally recurrent gyres in different parts of the basin. Distinct westward propagation of these gyres occurs, together with amplitude changes. For the first time a Mersa-Matruh Gyre is successfully simulated due to the introduction of our heat fluxes at the air-sea interface. The seasonal thermocline is formed each summer, and a deep winter mixed layer is produced in the region of Levantine intermediate water formation. Deep water renewal does not occur, probably due to the climatological forcing used.

1. Introduction

The newest discoveries in the circulation in the Mediterranean Sea are the subbasin gyres, the intense mesoscale variability, the strong seasonal signal in the circulation, and the winter convection processes producing deep and intermediate waters in the basin. Progress in this area has come both from new observational programs and modeling efforts. The observational picture of the western basin general circulation is reviewed by Millot [1991] and its eastern counterpart by the *Physical Oceanography of the Eastern Mediterranean (POEM) Group* [1992]. The results of the regional numerical models of Heburn [1987], Malanotte-Rizzoli and Bergamasco [1989, 1991], and Beckers [1991] showed some agreement between the model simulations and the known features of the basin general circulation. The studies on the seasonal cycle for the entire basin were initiated by Stanev *et al.* [1989], and further progress was made by Pinardi and Navarra [1993] after increasing the horizontal and vertical resolution of the models.

The basin scale steady state surface circulation emerging from these observational and modeling studies can be shown

to be composed of four major structures, schematically represented in Figure 1. The first major structure is the surface Atlantic stream system, composed initially of the inflowing Atlantic water jet, entering from the Strait of Gibraltar. After the Alboran Sea this jet becomes the Algerian current, which departs from the North African coast, forming a smooth and large-scale anticyclonic meander in the center of the southern Algerian-Provencal basin. After crossing the Strait of Sicily, the Atlantic stream system occupies the southern part of the Ionian basin and is called the Ionian-Atlantic stream, following Robinson *et al.* [1991]. The Ionian stream becomes the mid-Mediterranean jet, which intensifies between the Rhodes and Mersa-Matruh Gyres. The second major structure consists of the Lyon and Rhodes Gyres, which are the northern basin cyclonic gyres in which deep and intermediate waters form. The third major structure consists of the other cyclonic gyres of the basin, such as the Tyrrhenian Gyre, the western Ionian cyclonic gyre, and the cyclone southwest of Crete. Finally, the fourth major structure consists of the southern Mediterranean anticyclonic gyres such as the Alboran Gyre, the Mersa-Matruh Gyre, the Shikmona Gyre, and the northern Mediterranean (north of $\sim 37^\circ\text{N}$) anticyclones like the Pelops Gyre. Even more schematically, the basin circulation could be characterized by cyclonic gyres in the northern regions while anticyclonic gyres dominate the southern part of the basin. In our definition the northern regions consist of the northern Algerian-Provencal basin and the Tyrrhenian and the eastern Mediterranean areas north of 34°N . Both the

¹Permanently at Department of Meteorology and Geophysics, University of Sofia, Sofia, Bulgaria.

²Permanently at Ente per le Nuove Tecnologie, l'Energia, e l'Ambiente, Centro Ricerche Energia, Casaccia, Rome, Italy.

Copyright 1995 by the American Geophysical Union.

Paper number 95JC00233.
0148-0227/95/95JC-00233\$05.00

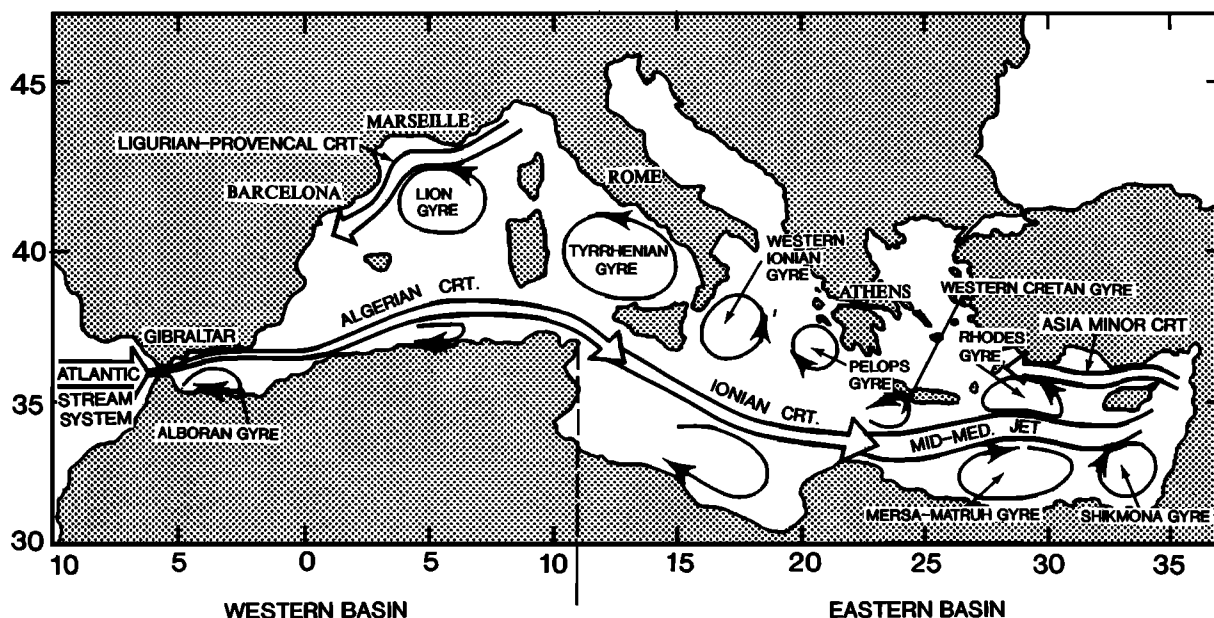


Figure 1. Schematic of surface circulation features in the Mediterranean basin.

cyclonic and anticyclonic gyres seem to be persistent throughout the water column, even though they are surface intensified. Other features reverse direction with depth, as is the case of the Atlantic stream at the Sicily Strait, which at ~200–300 m flows westward, carrying eastern Mediterranean (EM) waters into the western Mediterranean (WM) basin. Because of data scarcity the seasonal variability of this current system has not been fully explored. The only work that tried to assess the seasonal variability from the observational evidence is offered by *Tzipermann and Malanotte-Rizzoli* [1991] (hereinafter referred to as TMR). They find that the seasonal signal is confined to the surface (0–300 m) and that it is stronger in the eastern than western Mediterranean. In this paper we try to define the characteristics of the seasonal cycle using model simulations and to compare the results to TMR. An equivalent attempt was made by *Zavatarelli and Mellor* [1995] but with a different model and forcing.

Part of the seasonal variability of the basin is represented by the water formation processes occurring in the basin. This is a midlatitude basin where deep waters form like they do in the polar regions of the world ocean, presumably driving the basin circulation in a very important way. The deep waters of the WM are formed in the Lyon Gyre [*Madec et al.*, 1991], while for the EM the source is probably localized entirely in the southern Adriatic region [*Roether and Schlitzer*, 1991]. The deep water formation processes are associated with winter shelf and open ocean convection chimneys [*Jones and Marshall*, 1993], which produce the pool of deep waters in the two basins. The main thermocline water masses of the Mediterranean, located at ~300–500 m, are composed of salty waters called Levantine intermediate waters (LIW), formed during winter in the Levantine basin. The region of major production of these waters is probably the Rhodes Gyre, and the process seems to be associated with nonpenetrative convection in the mixed layer [*Ozsoy et al.*, 1991; *Lascazatos et al.*, 1993]. *Miller* [1983] shows that

the climatological depth of the LIW core is 300 m in the EM and 400–500 m in the WM.

In the present paper we study the seasonal variability of the Mediterranean basin circulation as simulated by a general circulation model (GCM) driven by climatological forcings. The GCM used is the Geophysical Fluid Dynamics Laboratory modular ocean model (GFDL-MOM) [*Pacanowski et al.*, 1990], implemented in the Mediterranean area with a sophisticated parameterization of the heat budget at the surface. The heat and wind fluxes are interactively calculated by the model, which receives as input the “raw” atmospheric fields, such as the National Meteorological Center (NMC) analyses at 1000 hPa. This is one of the novelties of this model application: We developed “realistic” air-sea physics for a climatological integration of the model. We will see in section 3.4 that this implies a climatic drift of the model, and we will discuss some of the problems.

The main focus of this study is the investigation of the ocean response to a monthly varying climatological forcing, called a “perpetual year” forcing. Even though this forcing is unrealistic because of the large synoptic and interannual variability of the atmospheric parameters in the Mediterranean area, we think that this could define the fundamental characteristics of the seasonal circulation of the basin. The model has been integrated for a long time (about 70 years) to obtain the “typical” seasonal circulation of the basin. The analysis of the model simulations will concentrate upon the water transformation processes occurring in different regions of the basin and the changes in the barotropic and baroclinic structure of the subbasin gyres due to the seasonal components of the Mediterranean forcing parameters. Comparison with TMR observational results will be discussed throughout the paper.

In section 2 we describe the model design and the atmospheric forcing parameterizations. In section 3 the barotropic and baroclinic components of the seasonal cycle are discussed, together with the sensitivity experiments to dif-

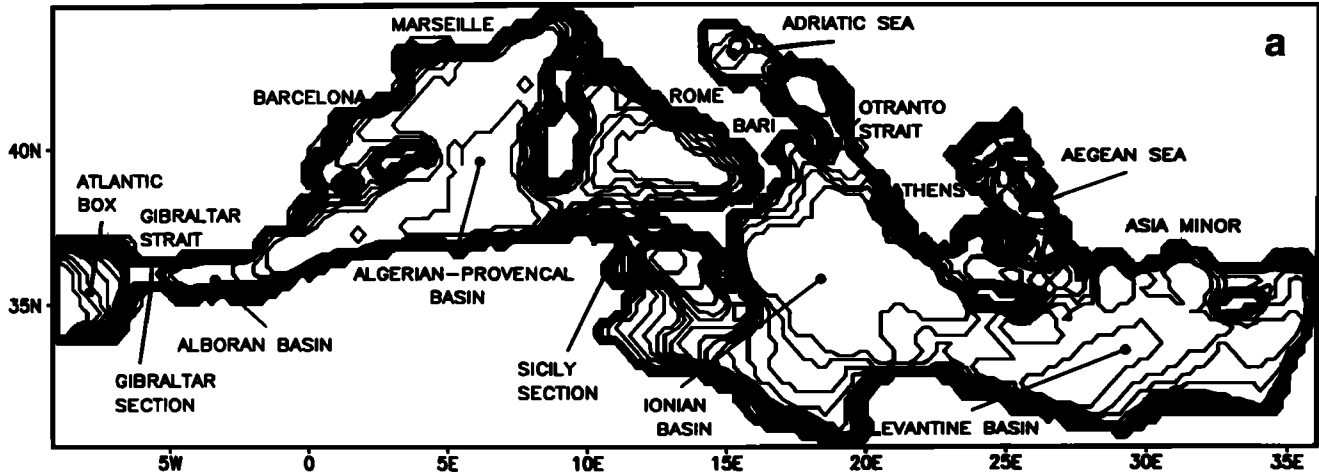


Figure 2. (a) Model geometry and levels. The isolines indicate model levels. (b) Schematic of model level positions and thicknesses.

ferent atmospheric forcing parameterizations. The last section provides the conclusions.

2. Model Design

2.1. Model Equations

The model geometry and topography for the choice of vertical and horizontal grid spacing of the model are shown in Figure 2a. The model levels are shown in Figure 2b. The horizontal resolution is $\frac{10}{4} \times \frac{10}{4}$ in latitude and longitude. West of the Gibraltar Strait there is a box of about $3^\circ \times 3^\circ$ degrees inside the North Atlantic which will be used to impose the inflow of Atlantic waters into the Mediterranean; this will be discussed in section 2.3.

This choice of model geometry allows us to define the Alboran, Provencal-Algerian, and Tyrrhenian basins (see Figure 2a) in the western Mediterranean and the Ionian and Levantine basins in the eastern Mediterranean. The Adriatic basin is cut in the middle since its very shallow northern area would not be adequately resolved by the model. Several islands have been lumped together in the Aegean Sea because of the horizontal resolution. The straits of Kithira and Kassos-Karpathos on the western and eastern part of Crete have been enlarged, the island of Rhodes has been connected to the mainland, and the islands of Kassos and Karpathos have been submerged.

The model equations, written in spherical coordinates (λ , φ , and z), are

$$\frac{\partial \mathbf{u}_h}{\partial t} + \mathcal{L}(\mathbf{u}_h) - \frac{mn}{a} u(\hat{k} \times \mathbf{u}_h) + \mathbf{f} \times \mathbf{u}_h = -\frac{1}{\rho_0} \nabla p - A_h \nabla^4 \mathbf{u}_h + A_v \frac{\partial^2 \mathbf{u}_h}{\partial z^2} \quad (1)$$

$$p_z = -\rho g \quad (2)$$

$$\mathcal{L}(1) = 0 \quad (3)$$

$$\frac{\partial T}{\partial t} + \mathcal{L}(T) = -K_h \nabla^4 T + K_v \frac{\partial^2 T}{\partial z^2} + \alpha_T(x, y, z)(T - T^*) \quad (4)$$

$$\frac{\partial S}{\partial t} + \mathcal{L}(S) = -K_h \nabla^4 S + K_v \frac{\partial^2 S}{\partial z^2} + \alpha_S(x, y, z)(S - S^*) \quad (5)$$

$$\rho = \rho(T, S, p) \quad (6)$$

where $\mathbf{u} = (u, v, w)$ is the velocity vector and \mathbf{u}_h its horizontal component, $\mathbf{f} = 2\omega \sin(\varphi)\hat{k}$, \hat{k} is the unit vector in the z direction, $n = \sin(\varphi)$, $m = \sec(\varphi)$, p and ρ are the pressure and density, T and S are the temperature and salinity fields, respectively, and the advection operator $\mathcal{L}(\mu)$ is defined as

$$\mathcal{L}(\mu) = \{\sec(\varphi)a^{-1}[(u\mu)_\lambda + (v\mu/\sec(\varphi))_\varphi] + (w\mu)_z\}. \quad (7)$$

Here a is the radius of Earth and the subscripts indicate partial differentiation. The time step used is 3600 s for the tracer and momentum equations. The coefficients of turbulent diffusion are $A_h = 8 \times 10^{18} \text{ cm}^4/\text{s}$, $K_h = 2.4 \times 10^{19} \text{ cm}^4/\text{s}$, $A_v = 1.5 \text{ cm}^2/\text{s}$ and $K_v = 1 \text{ cm}^2/\text{s}$. These values were chosen after some sensitivity studies were performed. It turned out that for the cases of Laplacian mixing with $A_h = 4 \times 10^6 \text{ cm}^2/\text{s}$ and $K_h = 1.2 \times 10^7 \text{ cm}^2/\text{s}$ and our biharmonic mixing coefficients (see also Cox [1985]), the volume mean kinetic energy reaches almost the same values after the periodic solution is obtained. The coefficient of vertical diffusion was chosen small enough so as not to create unrealistically strong mixing in the deep layers but high enough to allow for downward penetration of heat during the seasonal cycle. In our experiments we varied K_v in the range from 0.1 to $1 \text{ cm}^2 \text{ s}^{-1}$, and we chose the latter because it allowed a reasonable steepness in the seasonal thermocline at the surface.

Equation (6) is the Unesco equation of state for sea water. Convection is introduced into the model using the procedure proposed by Bryan [1969]. In case of static instability the temperature and salinity of the unstable column are locally homogenized until neutral stratification is reached.

The α terms in (4) and (5) are the Newtonian restoring terms which are different from zero only in selected regions of the model. In particular, at the first model level (5 m)

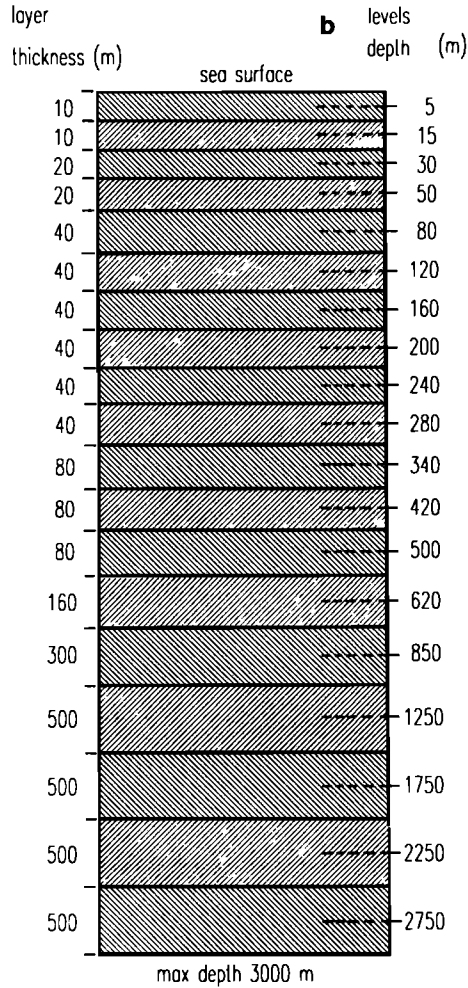


Figure 2. (continued)

$$\alpha_S = 0.2 \text{ d}^{-1},$$

$$\alpha_T = 0,$$

and for all the other levels and only between $9.5^\circ\text{W} < \lambda < 6.5^\circ\text{W}$ (the Atlantic box)

$$\alpha_T = \alpha_S = 0.2 \text{ d}^{-1}$$

In the region of the Atlantic box and below the surface, the reference temperature and salinity fields T^* and S^* are the annual mean *Levitus* [1982] climatologies.

The specification of salt fluxes at the sea surface is generally related to the problem of prescribing precipitation-evaporation (P-E) values. The lack of data for precipitation in open sea areas makes almost impossible the evaluation of the real sea surface water fluxes, or in particular their seasonal variations. We solved this problem by imposing the salinity structure at the first model level, as indicated by (5). The S^* at this level was obtained from an objective analysis of National Oceanographic Data Center (NODC, Washington, D. C.) climatological casts for the Mediterranean area (kindly made available to us by S. Levitus). A monthly mean field was then obtained using the same procedure of *Levitus* [1982], but with finer horizontal grid spacing and some differences in the specification of the first guess field in the

objective analysis method [*Roussetov and Brasseur, 1991*]. On the basis of this monthly data set, the 5-m salinity field S^* is computed in the model at every time step using linear interpolation.

The model assumes the following boundary conditions at $z = 0$:

$$\rho_0 A_v \mathbf{u}_{hz} = \boldsymbol{\tau} \quad (8)$$

$$\rho_0 C_P K_v T_z = Q \quad (9)$$

$$K_v S_z = 0 \quad (10)$$

$$w = 0 \quad (11)$$

where $\boldsymbol{\tau}$ is the wind stress and Q is the net surface heat flux. The form of Q and $\boldsymbol{\tau}$ will be discussed in detail in section 2.2.

At the bottom $z = -H(\lambda, \varphi)$ the vertical velocity is imposed

$$w = -\mathbf{u}_h \cdot \nabla H \quad (12)$$

where the surface $z = H(\lambda, \varphi)$ is the bathymetry and

$$K_v(T_z, S_z) = 0. \quad (13)$$

The initial boundary value problem of (1)–(6) is solved starting from the annual mean *Levitus* [1982] T and S fields and zero initial velocity fields.

2.2. The Heat and Momentum Budget at the Surface

The energy budget at the sea surface was implemented following closely the formulation of *Rosati and Miyakoda* [1988] with the clear sky assumption. The net heat flux at the ocean surface Q was written as

$$Q = Q_s - Q_u \quad (14)$$

where Q_s is the downward flux of solar radiation and Q_u is the net upward flux of radiation emitted by the sea surface via radiative and evaporative-convective processes.

The downward flux can be expressed as

$$Q_s = Q_T(1 - 0.62C + 0.0019\beta)(1 - \alpha) \quad (15)$$

where C is the fractional cloud cover which in the present study is chosen to be zero; $\beta(\varphi, d)$ is the solar noon altitude in degrees which is a function of the Julian day d and the latitude φ ; and α is the sea surface albedo chosen to be constant and equal to 0.3. The total radiation reaching the surface under clear skies

$$Q_T = J_0 a^{-2} \cos(\xi) D_F(\varphi, \lambda) [\tau^{\sec(z)} + (1 - A_\alpha)]/2 \quad (16)$$

depends on the atmospheric attenuation and scattering, controlled by the transmission coefficient $\tau = 0.7$, the zenith angle ξ , the water vapor and ozone absorption $A_\alpha = 0.09$, the solar constant $J_0 = 1.35 \times 10^3 \text{ J m}^{-2} \text{ s}^{-1}$, and the fraction of daylight D_F . The net upward flux of energy from the surface is composed of the net flux of longwave radiation lost by the sea surface Q_B and sensible H_a and latent LE_a heat fluxes

$$Q_u = Q_B + H_a + LE_a \quad (17)$$

where L is the latent heat of vaporization (2.501×10^6 J kg^{-1}). We used the following bulk parameterization formulas:

$$Q_B = \varepsilon \sigma T_s^4 [0.39 - 0.05 r e_{\text{sat}}^{1/2}(T_a)] + 4 \varepsilon \sigma T_s^3 (T_s - T_a) \quad (18)$$

$$H_a = \rho_a C_p C_h |\mathbf{W}| (T_s - T_a) \quad (19)$$

$$E_a = \rho_a C_e |\mathbf{W}| [e_{\text{sat}}(T_s) - r e_{\text{sat}}(T_a)] (0.622 / p_a) \quad (20)$$

where T_s and T_a are the sea surface temperature and the atmospheric temperature at 1000 hPa, respectively, ε is the emissivity of the sea ($\varepsilon = 0.97$), σ is the Stefan-Boltzmann constant, r is the relative humidity, $e_{\text{sat}}(T)$ is the polynomial approximation of the saturation water pressure, as given by *Lowe* [1977], ρ is the density of the air, p_a is the surface air pressure (1013 hPa), $|\mathbf{W}|$ is the surface winds amplitude, C_p is the specific heat capacity (1.005×10^3 J kg^{-1} K^{-1}), and C_h and C_e are the turbulent exchange coefficients (1.1×10^3).

The momentum flux is given by the wind stress components

$$(\tau^\lambda, \tau^\varphi) = \rho_a C_D |\mathbf{W}| (W_x, W_y) \quad (21)$$

where W_x , W_y are the wind components. The polynomial approximation, given by *Hellerman and Rosenstein* [1983], is used to calculate the drag coefficient C_D as a function of the wind speed W and $(T_a - T_s)$. Both momentum and heat fluxes are calculated interactively: the model calendar is set to correspond to the real time of the atmospheric data set; the atmospheric data are interpolated at every time step; and the model time is used to calculate the solar radiation at every grid point.

The value of Q_s is averaged over a day for each grid point and is kept constant each day, and the value of T_s in all parameterization expressions for the wind stress and heat flux is set to be equal to the current model sea surface temperature.

The required atmospheric quantities to calculate (15)–(21) are the wind field \mathbf{W} , the atmospheric temperature T_a , and the relative humidity r . They were derived from the 12-hour NMC 1000-hPa operational analyses for the period January 1980 through December 1988. From this data set we calculated a climatology or perpetual year of atmospheric parameters by computing the monthly average of the time series.

In Figure 3a we show the wind stress calculated by the model, imposing the average \mathbf{W} and T_a and using the parameterizations written in (21). We recognize the Mistral area in the northwestern Mediterranean basin and a zonal stress over the whole eastern basin during winter. The spring-to-summer conditions are characterized by the well-known change in wind stress direction in the eastern Mediterranean area, giving rise to a northwesterly stress over the Aegean and Levantine basin (Etesian winds). Overall, this climatological wind stress pattern is similar to the traditional climatological wind stress of *Hellerman and Rosenstein* [1983] (hereinafter referred to as HR), but with significant differences, especially in the magnitude of the wind stress. The amplitude of the Mistral is greatly reduced with respect to HR [see *Pinardi and Navarra*, 1993], but the summer Etesian wind stresses are larger in amplitude. Furthermore,

the NMC wind stresses are more zonal than HR and generally weaker during winter. This is probably due to the short length of the time series used to compute the climatological forcing parameters (only 9 years) as compared to HR. *Heburn* [1994] discusses at length the differences between HR and European Centre for Medium-Range Weather Forecasts (ECMWF) data averaged over an analogous period of time (1981–1989). He finds that interannual variability is so large that the average of the wind stress over this period of time gives a different magnitude of τ but the patterns generally agree. The NMC data also show a very large interannual variability, as shown by *S. Castellari et al.* (A heat budget study for the Mediterranean Sea, submitted to *Oceanologica Acta*, 1995; hereinafter referred to as *Castellari et al.*, submitted manuscript, 1995).

In Figure 3b we show the wind stress curl for the stresses of Figure 3a. The summer-to-winter changes are noticeable over large portions of the basin, such as the Algerian-Provencal and the Ionian areas. During the winter and autumn seasons the wind stress curl shows a zero crossing line along the central latitude of the two basins, dividing the negative southern from the positive northern wind stress curl areas of the Mediterranean basin. This is due to the zonality and jetlike structure of the wind stress during winter and autumn, which produces a dipolar structure in the wind stress curl across the north-south extension of the basin. Taking a Sverdrup balance for the barotropic part of the flow field, we expect the northern areas to be forced with cyclonic vorticity while the south is driven with anticyclonic vorticity. In the WM the seasonal changes consist of a weakening of the amplitude of the wind stress curl over large areas of the basin with a weak summer reversal in the northern Provencal-Algerian basin. In the EM the seasonal changes are very large over the Ionian basin, where the wind stress curl changes from a dipolar structure during November and February to a negative wind stress curl over the whole basin in August. The northern Levantine basin is instead forced all year long with a cyclonic vorticity input. The southern Levantine wind stress curl is quite variable but generally consistent with a negative (anticyclonic) vorticity input. The dipolar structure of the wind stress curl is a common feature of the basin winds, as can be seen from the previous work of *Heburn* [1987] and *Pinardi and Navarra* [1993]. The major differences in curl between Figure 3b and HR [see *Pinardi and Navarra*, 1993] are in the southern part of the basin, where small-scale structures are evident in HR and not in NMC. Furthermore, the double-center structure of HR in the Mistral area is weaker, if not absent, in NMC and much more seasonal.

In Figure 3c we show the climatological Q computed by the model. The winter and autumn heat loss almost balances the net heat gain during spring and summer. If we compute a basin (east of Gibraltar) and yearlong average of Q , we obtain -0.4 W/m^2 , which balances the positive net heat transport at Gibraltar. This heat transport is clearly underestimated at Gibraltar since it should be close to 7 W/m^2 . This is probably due to the model's systematic warming of the thermocline waters, which reduces the temperature contrast at Gibraltar and thus the net heat transport. The striking feature of the pattern of Q in Figure 3c is its boundary structure during all the seasons, except perhaps winter. The summer local maxima along the eastern coast-

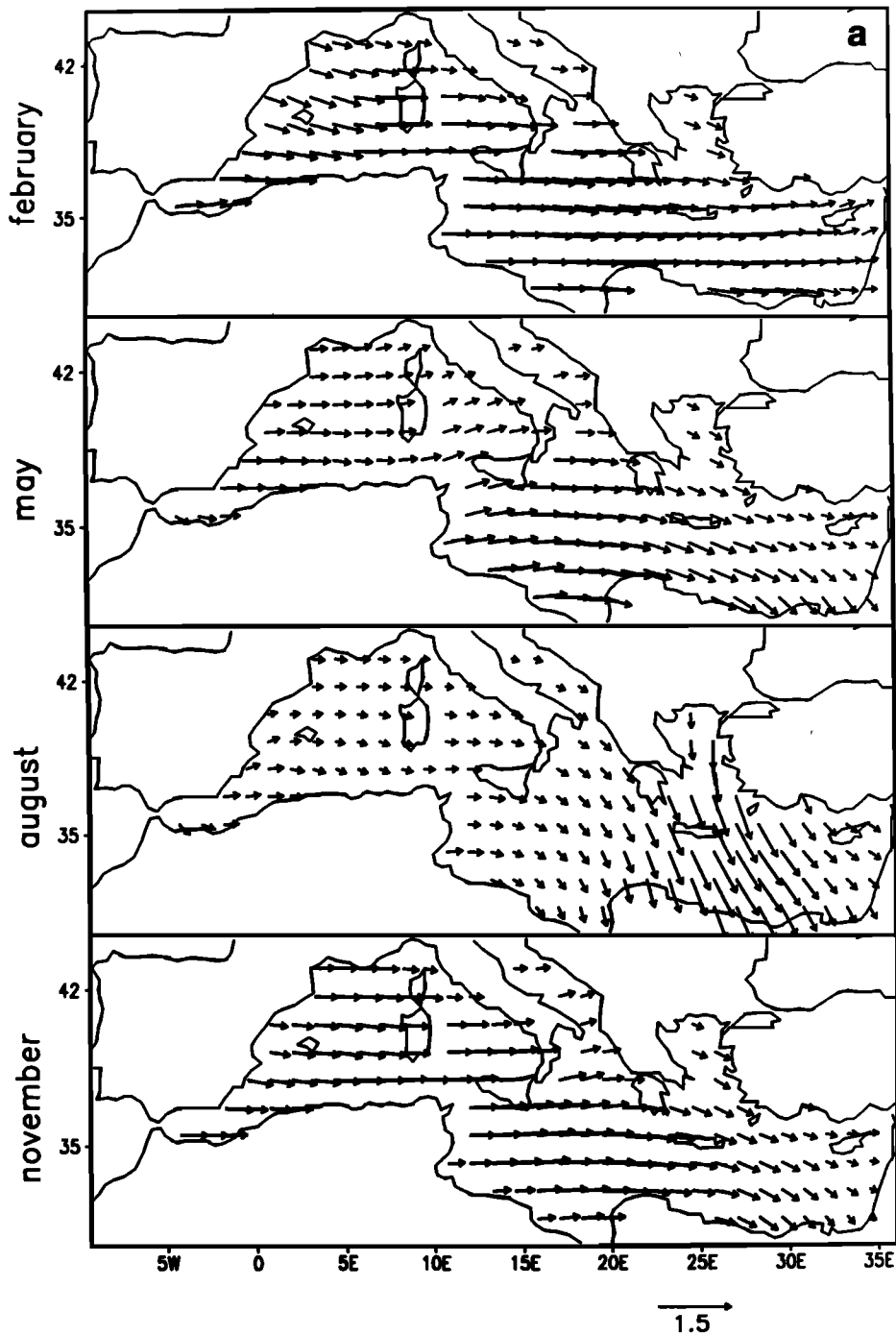


Figure 3. PY2 experiment: (a) Wind stresses. The units are dynes per square centimeter, and maximum values are 0.9 dyn/cm^2 during winter. (b) Vertical component of the wind stress curl in units of 10^{-9} dyn/cm^3 . (c) Total heat flux Q at the model surface in watts per square meter.

lines of the basin (eastern Tyrrhenian, Adriatic, and Aegean Seas) and south of Sicily are due to intense upwelling processes occurring there. The summer minima along the Algerian coasts and the southeastern Mediterranean coastlines could be due to downwelling motion generally occurring there. It is interesting to note that a local maximum of heat gain, which should correspond to upwelling areas, is evident along the western part of the Gulf of Syrte, the Tunisian coast, which is a known area of regional upwelling.

The downwelling and upwelling motion along the different parts of the coastlines is inferred by inspecting the upper water column horizontal velocity divergence (not shown here) and assuming conservation of mass. During winter these downwelling areas correspond to maximum values of heat loss. The southern part of the basin is an important heat release region during winter as well, as some of the eastern sides of the basin correspond to heat gain regions during summer. This boundary-intensified response to atmospheric

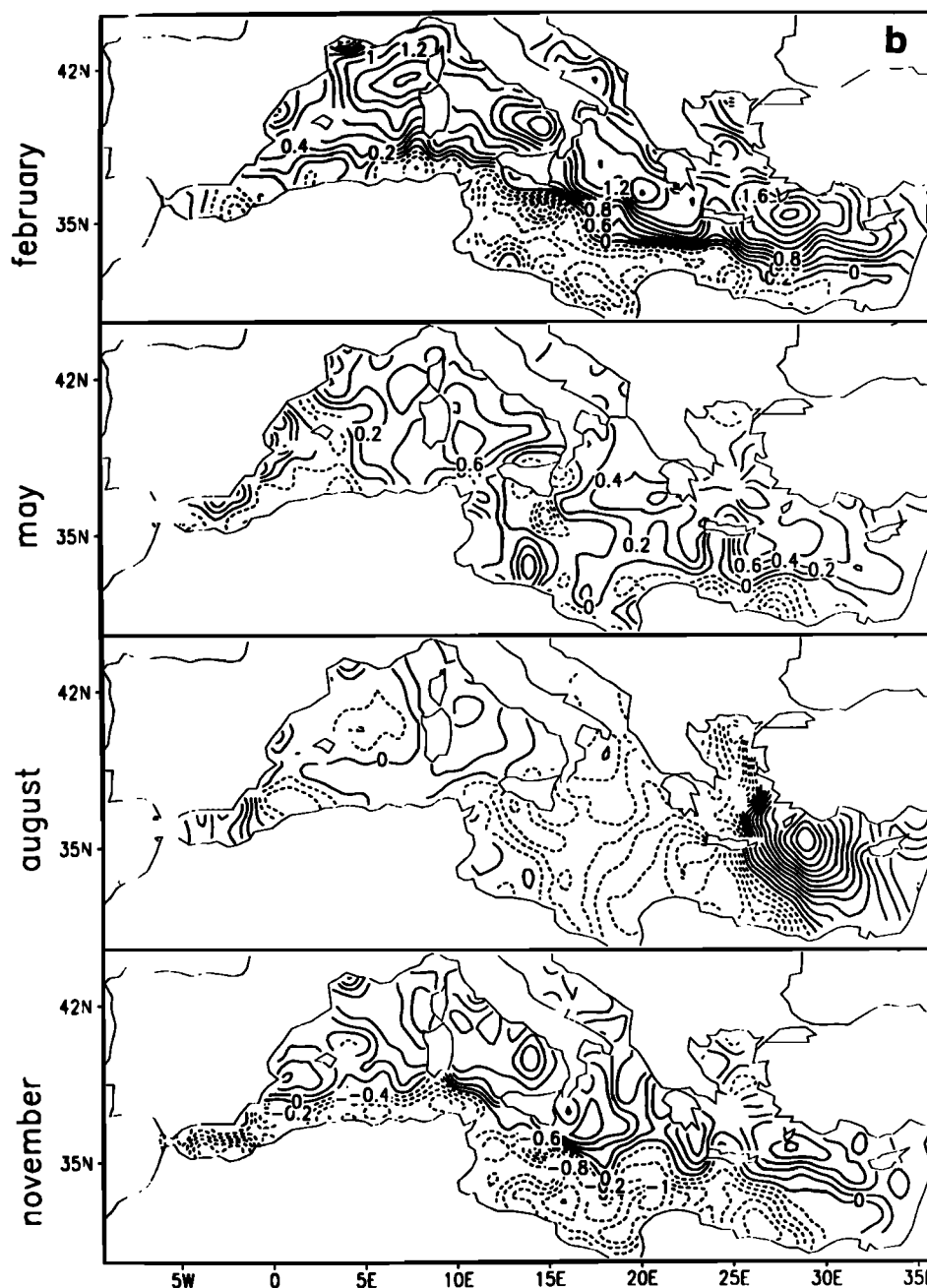


Figure 3. (continued)

heat forcing seems to be consistent with the observations (Castellari et al., submitted manuscript, 1995), at least during winter and in the summer upwelling regions.

2.3. The Strait of Gibraltar

Another model development is concerned with the addition of the Strait of Gibraltar inflow-outflow system. A problem is that the resolution in the Straits should be substantially increased compared to the open ocean regions in order to resolve the specific dynamics of the area. However, our model resolution is clearly too coarse to effectively resolve Gibraltar (~ 20 km at the narrowest point), so we had to increase the actual extension of the

Strait in order to fit two u , v grid points and be able to compute the balances in the Strait.

West of the Strait of Gibraltar the model area was extended up to 9.5°W . In this relatively small area the α restoring terms of (4) and (5) are different from zero at all the levels. This maintains the baroclinic flow field near the climatological mean in the area of the Atlantic west of Gibraltar, thus forcing the inflow of Atlantic waters into the Mediterranean. This method has been widely used in other model simulations of the Pacific [Philander et al., 1987] and the North Atlantic [Bryan and Holland, 1989] to control areas of the model which are not well resolved. This is the first time that this procedure was applied near a strait in a

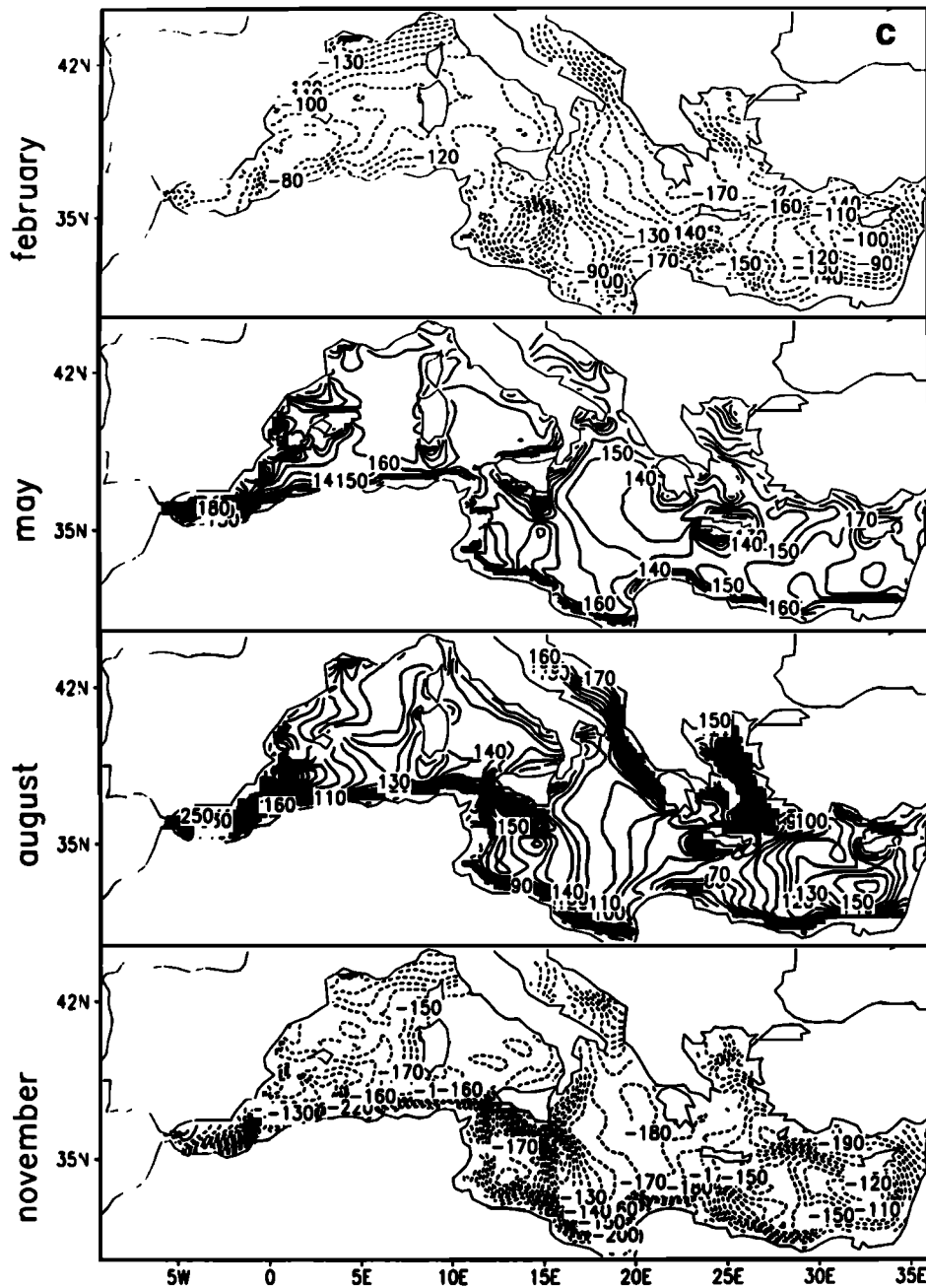


Figure 3. (continued)

large-scale model to try to fix the inflow conditions. On the outflow the constraint of the relaxation eliminates the need for strong damping of the variability emerging from the model predictions.

3. Simulation Experiments

In this section we present the analysis of the simulation experiments shown in Table 1. The central simulation is represented by experiment PY2 where all the forcings are considered together and the integration period was 67 years long. We will start by describing PY2 characteristics and comparing them with TMR observational evidence. In the last subsection we will compare PY2 with different forcing

experiments to show the robustness and sensitivity of the results to the model design.

In Figure 4 we show the volume-averaged kinetic energy for PY2. The model has reached a stable fully repeating cycle after about 50 years of integration. After a steep adjustment in the first 4–5 years of integration (not shown), a gradual change in the kinetic energy of the basin occurred, which took almost 50 years to stabilize. This is due to the adjustment of the model initial condition to the imposed atmospheric forcing and to the slow vertical diffusive adjustment of the first ~600 m of the water column. In Figure 4 the seasonal cycle is shown by two peaks: The largest is during the winter (March), and a smaller one is present for the summer (August). Superimposed on this seasonal cycle is a

Table 1. Simulation Experiments

Experiment	Heat and Salt Flux	Wind Stress	Gibraltar Strait	Duration of Experiment, years
HR	relaxation to annual mean temperature and salinity	monthly mean HR	open	7
NMC	relaxation to annual mean temperature and salinity	monthly mean NMC	open	7
GC	interactive heat flux and relaxation to monthly salinity	monthly mean NMC	closed	13
PY1	interactive heat flux and relaxation to monthly salinity	monthly mean NMC	open	13
PY2	interactive heat flux and relaxation to monthly salinity	monthly mean NMC	open	67

HR, *Hellerman and Rosenstein* [1983] winds; NMC, National Meteorological Center winds; GC, Gibraltar Strait closed; and PY, perpetual year experiments.

3-year-period interannual fluctuation. Later results, done with larger Atlantic boxes, have shown that the 3-year oscillation disappears, while the large seasonal cycle remains unaltered.

The absolute value of the mass transport at the Strait of Gibraltar is shown in Figure 5. The positive sign stands for inflow conditions at the Strait. The outflow is equal in amplitude but opposite in sign to the inflow because of the rigid lid assumption and the imposition of $\psi = 0$ along the continental coastlines. The seasonal variations of the mass transport of Figure 5 are weak, and they show a late winter and late summer peak, with an absolute minimum in January. This behavior is in very good agreement with the transport measurements of *Ovchinnikov* [1974]. The average value of 0.66 Sv is close to the measurement of 0.76 Sv reported recently by *Bryden et al.* [1988]. We believe our

results underestimate the measured transport but are not outside the possible values. The seasonal variations in transport are small (± 0.03 Sv). In the following section we will describe the barotropic and baroclinic components of the general circulation resulting from the PY2 experiment.

3.1. Barotropic Transport Components

The model solves the equations of motion by separating vertically integrated and baroclinic velocity components [*Bryan*, 1969]. The vertically integrated or barotropic velocity components (\bar{u} , \bar{v}) are horizontally divergenceless; for example, a horizontal mass transport stream function ψ can be defined, and then $\bar{\mathbf{u}} = \hat{k} \times \nabla\psi$, where \hat{k} is the unit vector in the vertical direction.

In Figure 6 we show the transport stream function fields for one of the repeating cycles of Figure 4. The flow field variability is different in the western and eastern basins since the response is composed by subbasin scale gyres. In the following we will describe the two regions separately.

1. The western Mediterranean basin shows the well-known cyclonic Lyon Gyre in the northern Provençal-Algerian basin. The seasonal variability of this gyre is represented by its weakening during summer, reaching minimum amplitude in September. The region south of the Atlantic stream is composed of small-scale gyres of anticyclonic nature. One of them is very intense and reaches maximum strength in late summer. The Tyrrhenian basin is composed of a large-scale cyclonic gyre during the winter, which is reduced in size and shifted westward during summer due to the westward propagation and strengthening of an anticyclonic gyre from the eastern side of the basin. This is the first example of a seasonally "recurrent gyre" for the Mediterranean basin, a feature which we think is very peculiar and fundamental to the basin barotropic general circulation. The results for the WM are in very good qualitative agreement with *Zavatarelli and Mellor* [1995], in both size and number of gyres found. These results are also similar to those of *Pinardi and Navarra* [1993] (hereinafter referred to as PN), except for the Algerian basin gyres. PN showed that during the summer an Algerian basin anticyclone was excited, while here the flow field shows only a

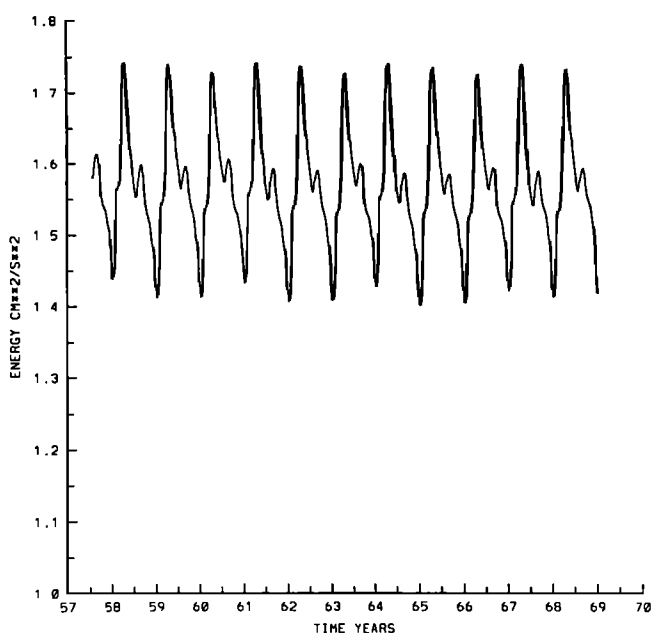


Figure 4. Volume integrated kinetic energy versus time for the last 10 years of experiment PY2.

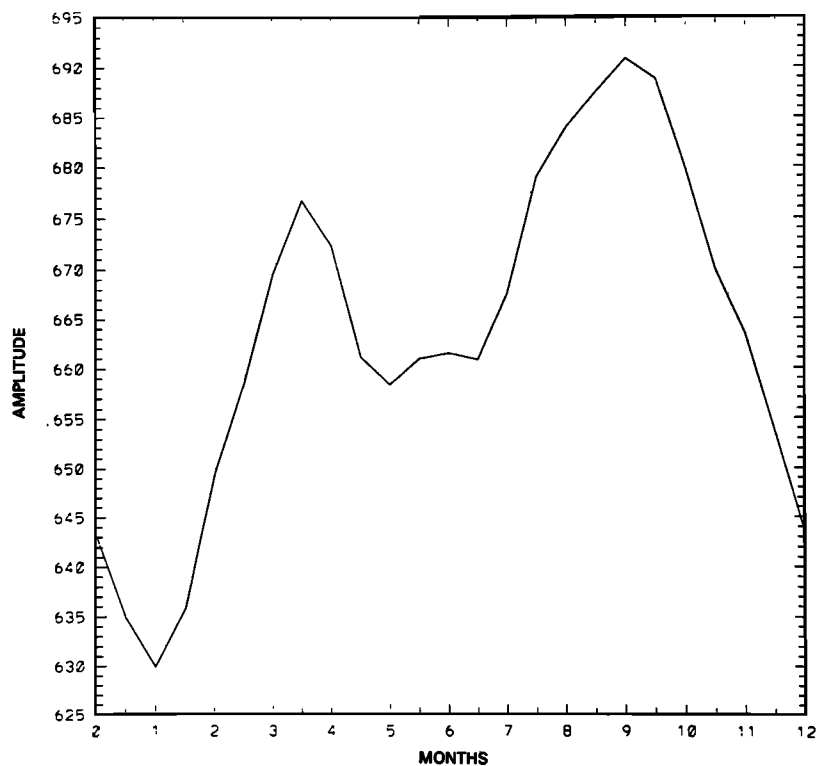


Figure 5. Absolute value of mass transport at the central longitude of the Strait of Gibraltar ($\sim 6^\circ\text{W}$) as a function of time for one of the seasonally repeating cycles in Figure 4. Units are sverdrups ($1 \text{ Sv} = 10^6 \text{ m}^3/\text{s}$).

very weak flow pattern during July–September. The disappearance of the large-scale anticyclone can be attributed to the Strait of Gibraltar control and to the different wind forcing used in this study with respect to PN. However, it is clear that the southern Provençal-Algerian basin is a region of anticyclonic motion for the barotropic components of the general circulation.

2. The eastern Mediterranean shows an overall cyclonic circulation in the basin connecting the Ionian and Levantine basins during winter, while during summer the circulation is composed of disconnected gyres of different sign. A major jetlike current, the barotropic component of the Atlantic-Ionian stream, is present from January until July, and its Levantine basin expression via the mid-Mediterranean jet is always recognizable. The northeastern Ionian basin reverses its circulation seasonally, giving rise to a recurrent anticyclonic gyre in the northern part of the Ionian. This definition of recurrent gyre is strictly seasonal, but we think that it could be related to the “interannual” recurrence that is described by *Robinson et al.* [1991]. In the central western part of the Ionian a cyclonic circulation persists throughout the year. PN showed a much more dramatic reversal of the Ionian circulation. Because of the westward propagating characteristics of the gyres, we think that the basic mechanism of Rossby mode propagation excited by wind stress changes is present also here. However, the response is different in shape and period, probably modified by the different representation of the wind stress curl and the bottom relief in this model. South of the Ionian-Atlantic stream the circulation is composed of different anticyclonic gyres, one of them clearly connected to the barotropic

component of the Mersa-Matruh Gyre. To our knowledge it is the first time that this gyre is simulated successfully, even though we are looking only at the barotropic response. It is interesting to observe the temporal behavior of the gyre: It is weak during the January–May period, and it reaches maximum strength in November (or the end of summer), splitting into two centers, one of them decaying in amplitude. The other novel and interesting result is the formation of an anticyclonic gyre under Cyprus, which clearly propagates westward and decays at the end of the summer. This is another example of a seasonally recurrent gyre. The Rhodes Gyre is another important feature of the basin circulation, which is positioned during January–March below the eastern corner of Crete. The barotropic expression of the Asia Minor current going around Cyprus and forming the northern border of the Rhodes Gyre is strong in the winter and spring seasons but weak in the others.

3.2. Baroclinic Flow Components

We describe now the baroclinic components of the general circulation from PY2. In Figure 7 we present the sea surface temperature (SST) predicted from the model. It is interesting to note the boundary-intensified signal of the SST, which in turn determines the boundary-intensified heat exchange with the atmosphere discussed before. The temperature range is from 15°C during winter and along the northern Mediterranean borders to 32°C in summer and along the southern Ionian basin. During winter (February) the most noticeable feature is the frontal structure in the EM, precisely along the Atlantic-Ionian stream path, which separates the warm waters of the African borders from the interior and northern

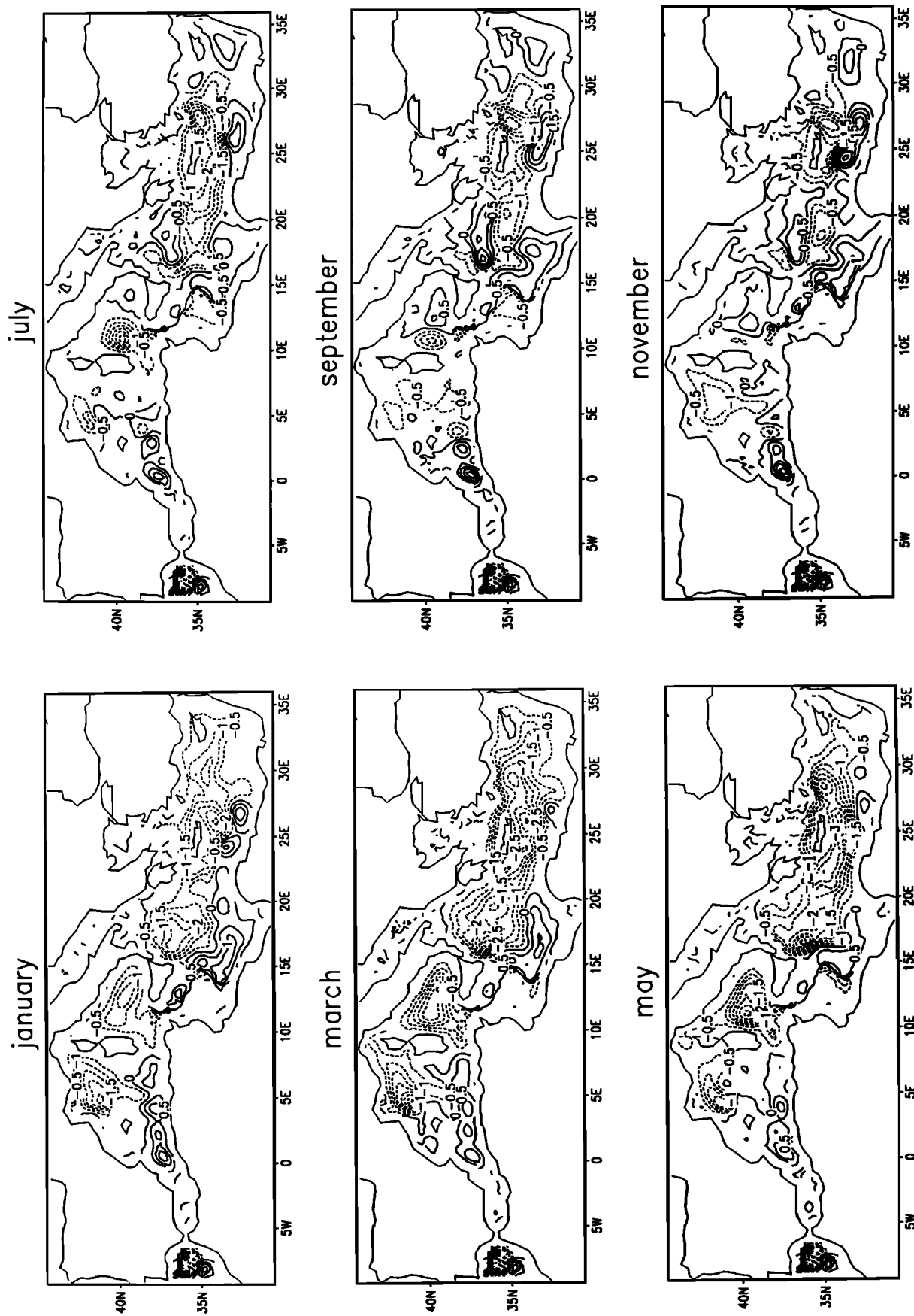


Figure 6. Snapshots of transport stream function at day 15 of different months inside one of the repeating cycles of Figure 4 (experiment PY2). Units are sverdrups. The month is indicated at the top of each profile.

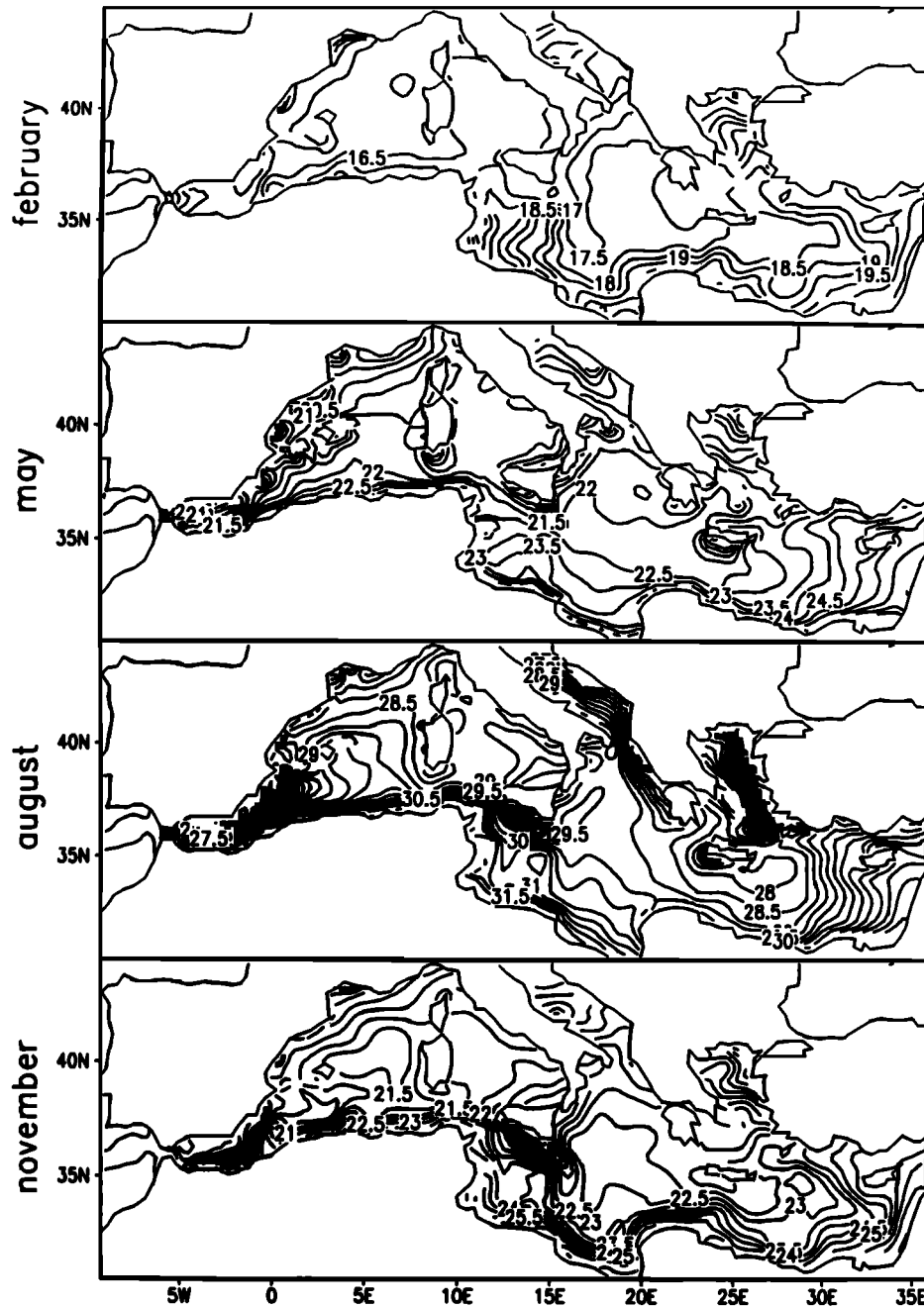


Figure 7. Sea surface temperature fields for one of the repeating cycles of Figure 4 (experiment PY2). Units are degrees Celsius and the month is written in the left margin of each profile.

cooler waters. The striking feature is the uniformity of the SST in the interior parts of the basin. The spring and summer months show the appearance of upwelling areas on the southern borders of the islands (Sicily and Crete) and along the eastern sides of the Adriatic and the Aegean.

In Figure 8 we show the temperature at different subsurface levels for the winter and summer months. The 50-m level was chosen because it marks the middle of the Atlantic water layer, and the 340-m level is well inside the LIW core for the EM. The structure at 50 m is practically identical to the SST of Figure 7, but at 340 m we start to see that the signature of the gyres and fronts differs from the sea surface temperature structures. In February the WM is dominated

by a southwest to northeast frontal structure in the middle of the Provencal-Algerian basin and by a meridional gradient at the southern border of the Tyrrhenian basin. The seasonal variability of the temperature fronts is clear in the Lyon Gyre area and in the Tyrrhenian basin.

In the EM and at 340 m there are three relevant structures: (1) the strong frontal structure south of the Otranto Strait, which separates the Adriatic Sea cold waters from the Ionian basin; (2) the Rhodes Gyre which shows seasonal fluctuations in shape and amplitude; and (3) the tongue-like structure emanating from the northeastern Ionian basin and changing the strength of the zonal temperature gradient in the Ionian between February and August. The southern Ionian basin

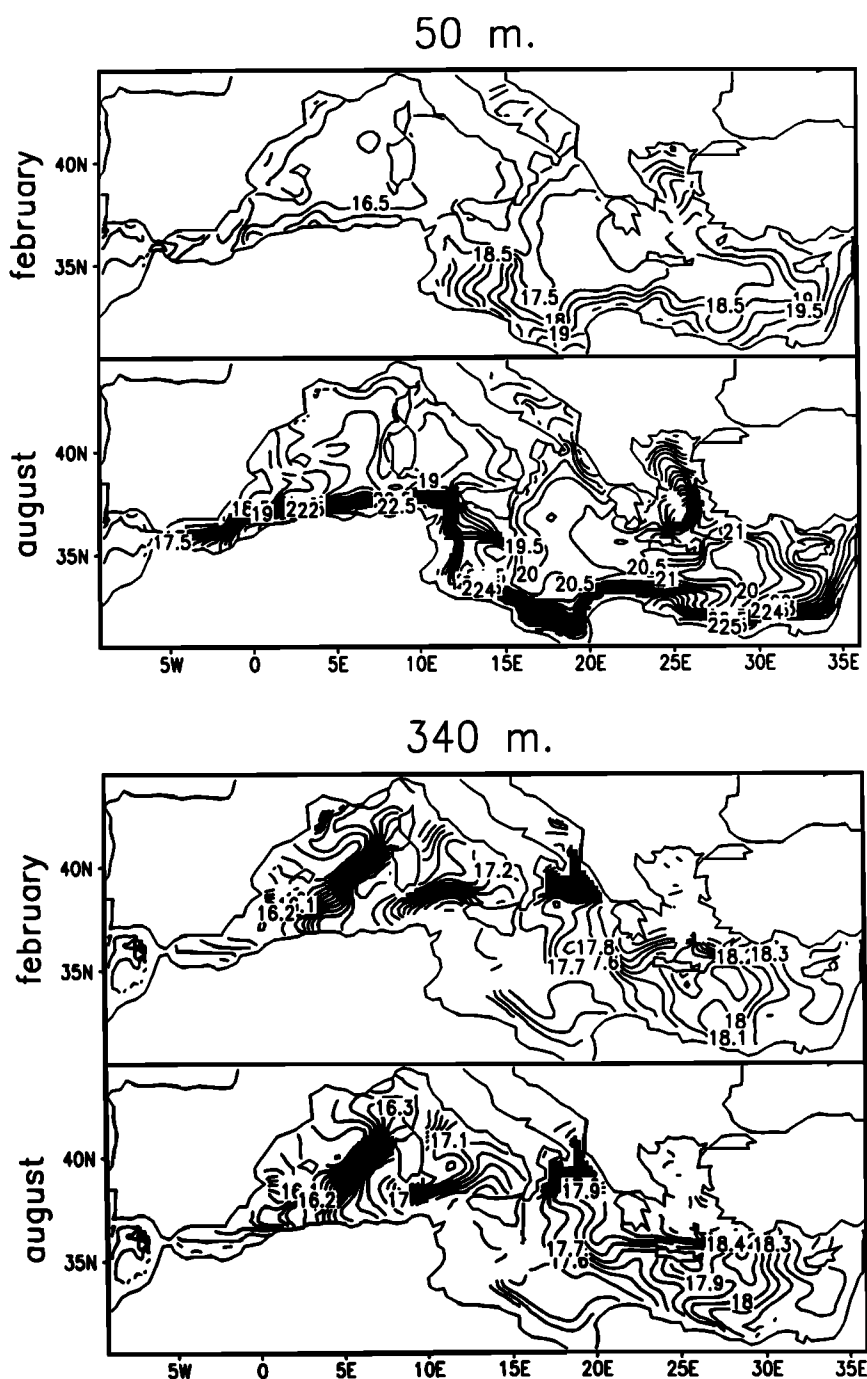


Figure 8. Snapshots of temperature in degrees Celsius for February and August at 50 and 340 m for one of the repeating cycles of Figure 4.

shows the shift of the 17.5°C isotherm a few degrees northward between February and August, decreasing the temperature frontal structure associated with the Ionian-Atlantic stream.

The salinity structure at the same depths is shown in Figure 9. The structures are similar to the temperature gradients described for Figure 8. At 50 m and in the EM it is interesting to note the signature of a salinity front under the surface position of the mid-Mediterranean jet which separates the saltier northern Levantine waters from the south. In the WM the LIW intrusion into the Tyrrhenian seems to

be stronger during August, where a tonguelike structure forms along the eastern border of the Tyrrhenian.

Finally, we have calculated the anomaly dynamic height at 100, 400, and 700 m, referred to as a 1700-m reference level (Figure 10). The anomaly is calculated with respect to a time and space average value of the dynamic height in the WM and EM separately. These profiles can be directly compared with the classical information on the general circulation of the basin as calculated from hydrographic data (see, for example, *Robinson et al.* [1991]). We will now describe the variability at the different levels.

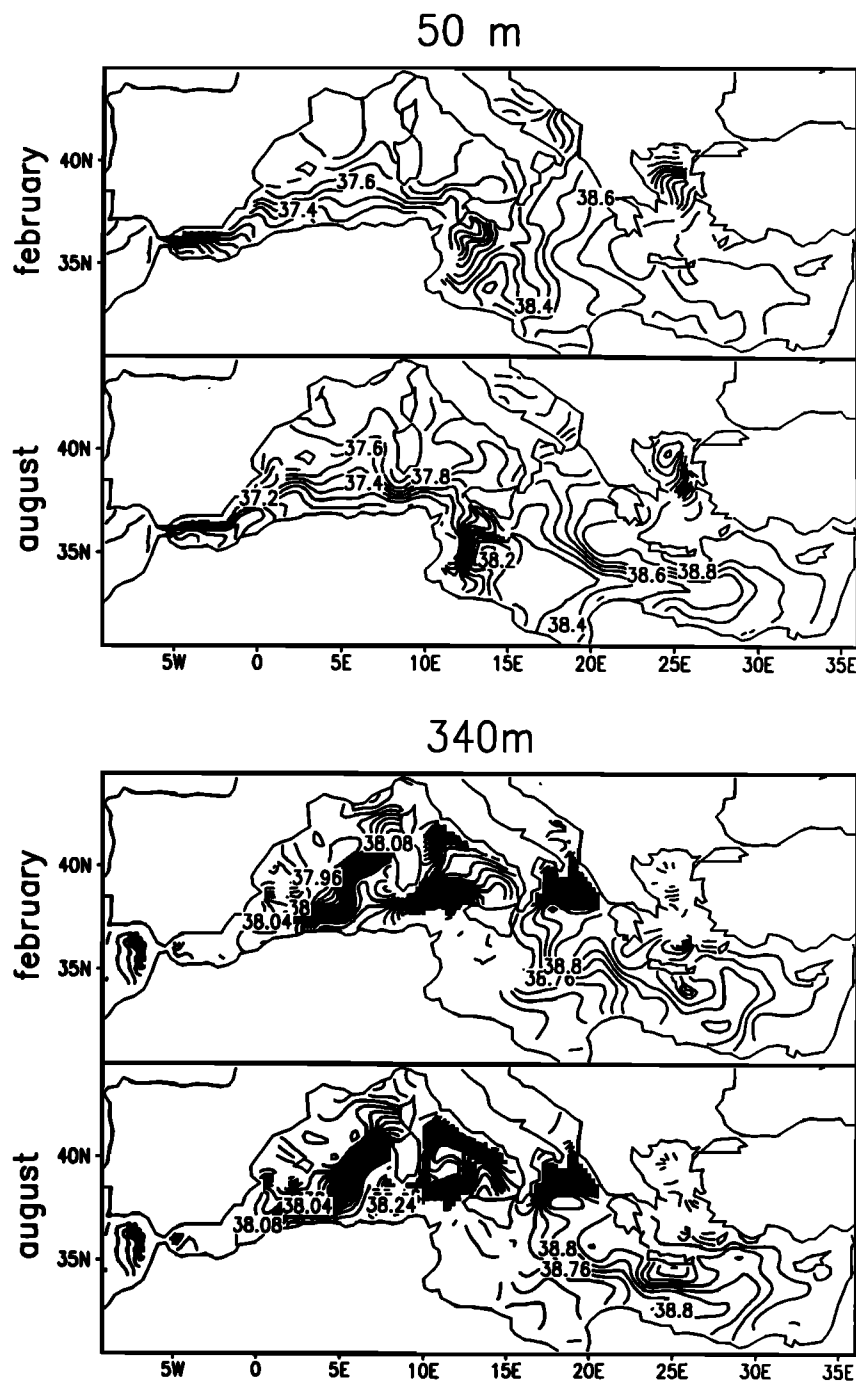


Figure 9. Snapshots of salinity for February and August at 50 and 340 m for one of the repeating cycles of Figure 4. Units are practical salinity units.

Variability at 100 m. The winter (March) dynamic height shows at this level a well-defined Atlantic stream system which winds along the southern part of the basin. The Algerian current is present in the jets around anticyclonic features on the right of the eastward flowing current. The Algerian current deviates from the coasts during the summer, and small anticyclonic gyres develop at the entrance of the current in the Algerian basin. The surface Lyon and Tyrrhenian cyclonic gyres are well positioned and reproduced by the model. The Ionian basin is divided longitudinally into two parts: The western part shows a persistent

cyclonic gyre and the eastern an anticyclonic area, near the Pelops Gyre of Figure 1. The Rhodes Gyre is strong, together with a clear signal of an Asia Minor current which hugs the Turkish coastline. The seasonal variability at this level is shown by a weakening of all the basin cyclonic gyres and the strengthening of the Mersa-Matruh Gyre during summer.

Variability at 400 m. It is at this level that maximum seasonal variability is achieved. The Algerian current is flowing westward, below the surface eastward flow, making a large anticyclonic meander in the Algerian basin. It seems

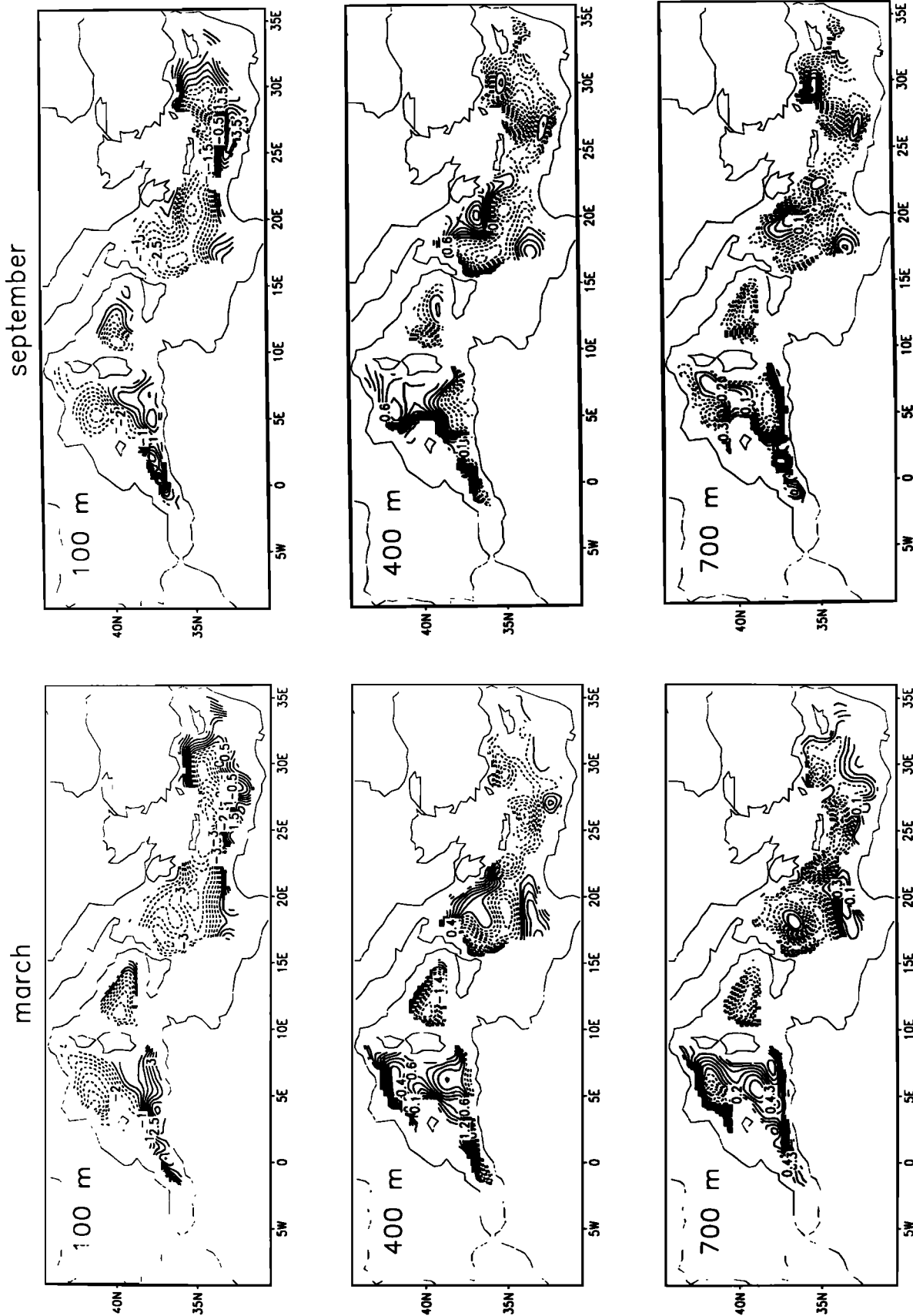


Figure 10. March and September PY2 dynamic height field at 100, 400, and 700 m, calculated with respect to a 1700-m reference level. Units are centimeters. An average value, *d.h.*, has been subtracted in the western and eastern basins separately: at 100 m, *d.h.* = -0.17 and -0.45 m for the western and eastern basins, respectively; at 400 m, *d.h.* = -0.26 and -0.47 m for the western and eastern basins, respectively; and at 700 m *d.h.* = -0.29 and -0.43 m for the western and eastern basins, respectively. Negative (dashed contours) and positive (continuous lines) anomalies stand for cyclonic and anticyclonic features, given a geostrophic balance.

that this current, bringing LIW from the eastern basin, branches south of Sardinia, and part of it goes directly toward the Alboran Sea while the rest joins the Lyon Gyre to the north. The Lyon Gyre is a well-defined feature at this depth throughout the year. The Tyrrhenian Gyre shows a partial reversal during summer. The eastern part of the basin is flowing anticyclonically during the summer, and a small but intense cyclonic gyre is left at the western side of the basin. In the EM the Ionian-Atlantic stream is present in segments around the intense subsurface gyre system. During summer the eastern Ionian area develops a well-defined anticyclonic gyre, similar to the Pelops Gyre of *Robinson et al.* [1991]. The summer-to-winter variability in the Levantine basin is large, with an amplification of the anticyclonic motion south of Cyprus. The Rhodes Gyre is formed by two cyclonic centers during winter and only one during summer, shifted westward with respect to the Rhodes deep basin. At this depth we see a well-defined Mersa-Matruh Gyre, which attains maximum amplitude during summer.

Variability at 700 m. During the winter and at the location of the surface Algerian current, a system of cyclonic and anticyclonic gyres of somewhat small scale is present. The seasonal variability of the gyres is large, showing a reversal of the Algerian anticyclonic gyre from summer to winter. The Lyon Gyre is always strong, while the Tyrrhenian Gyre partially reverses during summer. In the northern Ionian the western cyclonic gyre and an anticyclonic gyre are present in both summer and winter. The Rhodes Gyre center is broken down into two different cyclonic centers in winter, while in summer it is strong and displaced southward. The Mersa-Matruh Gyre is weak during February. As we could have expected, the deep circulation consists of a series of disconnected gyres, and the signature of the major current systems at the surface is present in the segments and jets around the intense gyre system.

In Figure 11a we show the PY2 velocity field for a climatological winter month (February) at 30 m, at the LIW level (300 m), and deeper (700 m). All the gyres present in the barotropic and baroclinic pictures shown above now merge in this winter velocity picture. In the WM the surface flow is dominated by the Algerian current meandering between Gibraltar and 4°E. Then the current splits into two branches, one flowing north and joining the Lyon Gyre, the other continuing along the Algerian coasts and entering the Sicily Strait. The Lyon and Tyrrhenian Gyres are well formed, but the Gulf of Lyon Gyre seems a little underestimated, probably due to the missing effect of deep water formation which should strengthen the cyclonic flow field in the upper water column. At the LIW depth the Algerian current is reversed, and the LIW flow entering from Sicily splits into three branches: one going into the Tyrrhenian, the second going along the western side of Sardinia, and the third continuing along the Algerian-Moroccan coastlines to outflow at Gibraltar. This is in agreement with the classical description by *Miller* [1983]. At 700 m the currents are more inhomogeneous, and they are consistent with the current directions at the surface, except along the Algerian coast. There is evidence of a small anticyclonic gyre west of Sardinia and along the Algerian coast which was present in the barotropic ψ field, and it emerges in the deep total velocity field here.

In Figure 11a and in the EM, we show a surface-intensified Ionian-Atlantic Stream and a western Ionian cyclonic gyre, a meandering mid-Mediterranean jet, and a well-developed

Asia Minor current throughout the water column. The Levantine basin shows a large-scale Rhodes Gyre at the surface and a rather well-developed Mersa-Matruh Gyre at 300 m. The deeper flow field is at a smaller scale, and it reverses in several subregions with respect to the 300-m level.

If we compare the 30-m and 700-m velocity fields with TMR winter analysis, we see that agreement in WM is very good, except perhaps in the Tyrrhenian, where, in our case, the western Tyrrhenian jet is closer to the coasts. In EM and in the Ionian, the general direction of currents is the same but the Ionian western gyre is smaller than TMR. The Ionian-Atlantic stream and mid-Mediterranean jet meandering pattern is well reproduced and consistent with TMR. In the Levantine, results generally agree but the noise in the data does not make possible a comparison, as also explained by TMR.

In Figure 11b we show the same velocity fields but for a summer month (August). In the WM and at the surface (30 m) the Algerian current is a well-developed current, as in winter. The Gulf of Lyon Gyre is still well defined but weaker than during winter. Large seasonal variations have occurred in the Tyrrhenian where the cyclonic gyre is now smaller, and the western Tyrrhenian current is now flowing in the middle of the basin. At 300 m the flow direction in the southern Algerian-Provencal basin is westward, and the flow entering from Sicily branches now only after Sardinia, probably taking first a whole turn around the Tyrrhenian basin. At 700 m the most noticeable difference with the 300-m flow field is the anticyclonic motion in the western Tyrrhenian Sea and the southward flow along the western side of Sardinia.

In the EM the Ionian-Atlantic stream branches into two segments in the Sicilian plateau, and the western cyclonic Ionian gyre is weak. At 700 m the central Ionian is occupied by an anticyclonic gyre, but the flow field along the western side of the basin is still directed southward. All of the southern part of the EM basin (south of 33°N) is occupied by anticyclonic gyres (Mersa-Matruh, Shikmona, and Syrte Gyres) which are much more intense than during winter. The Asia Minor current is now reversed at 700 m with respect to surface, and the Rhodes Gyre is a strong subsurface gyre feature.

If we compare 30- and 700-m velocities with the summer flow field of TMR, we see that again in the WM there is good agreement at the surface, except perhaps for the Tyrrhenian basin where we have a partial reversal of currents at 700 m. However, TMR also point out that in the Tyrrhenian there are large seasonal variations composed of a westward shift of the central Tyrrhenian jet. Our results are confirmed by the data analysis and modeling results of *Artale et al.* [1994]. In the EM and during summer, we find the largest differences with TMR analysis, the most evident being the anticyclonic gyre in the central Ionian basin. This could be due to model inadequacy in resolving topography, and further studies are needed to clarify the variability in this basin.

3.3. Water Mass Formation Processes

In this section we will describe a few cross sections of salinity and temperature in different regions of the basin in order to show the seasonal thermocline formation cycle in experiment PY2. The first section is across the whole longitudinal extension of the Mediterranean basin and is shown in Figure 12a. Starting with the temperature and from

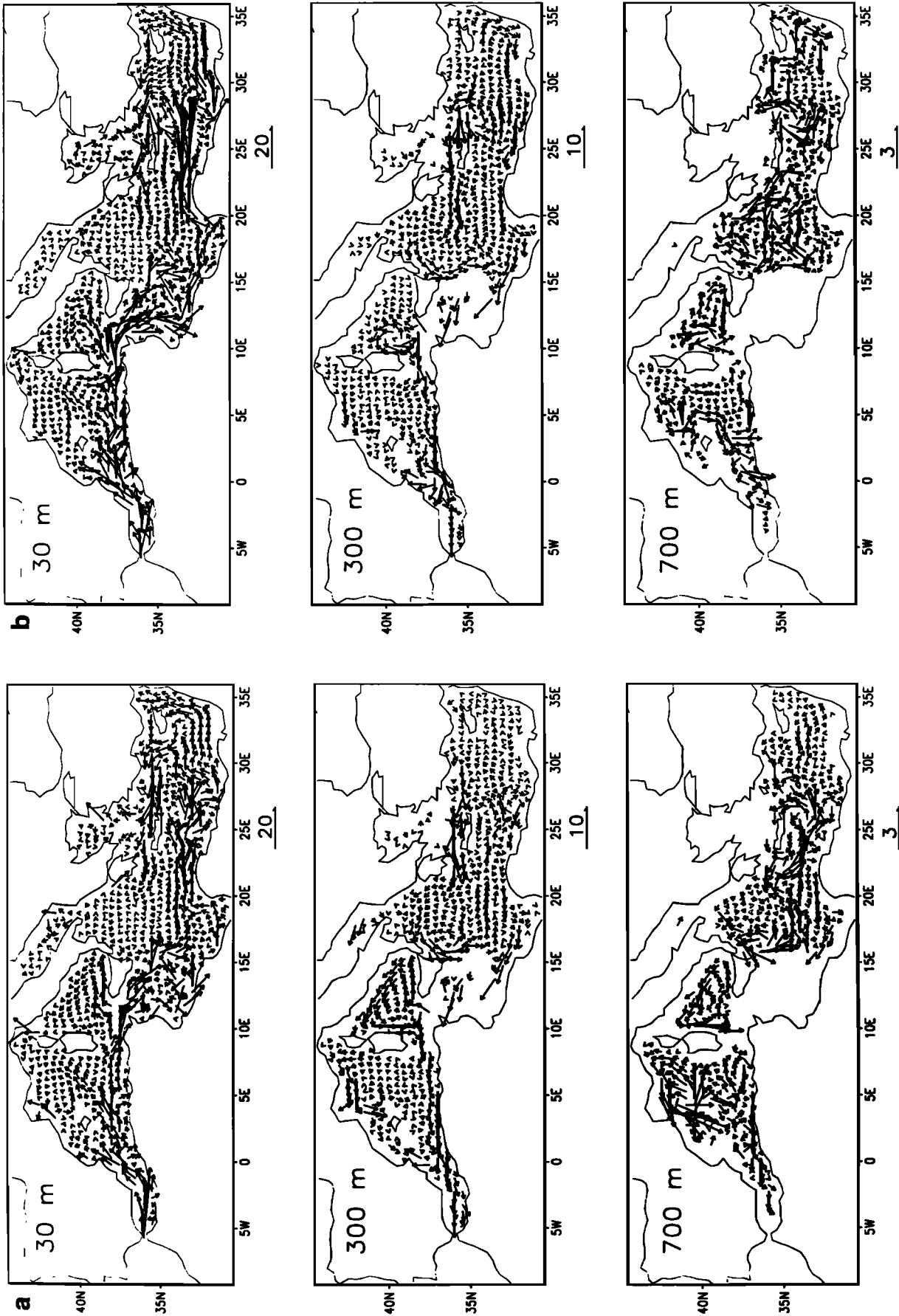


Figure 11. PY2 total velocity vectors for (a) February and (b) August at three depths (30, 300, and 700 m). The reference velocity arrow is indicated below the profiles, and units are centimeters per second.

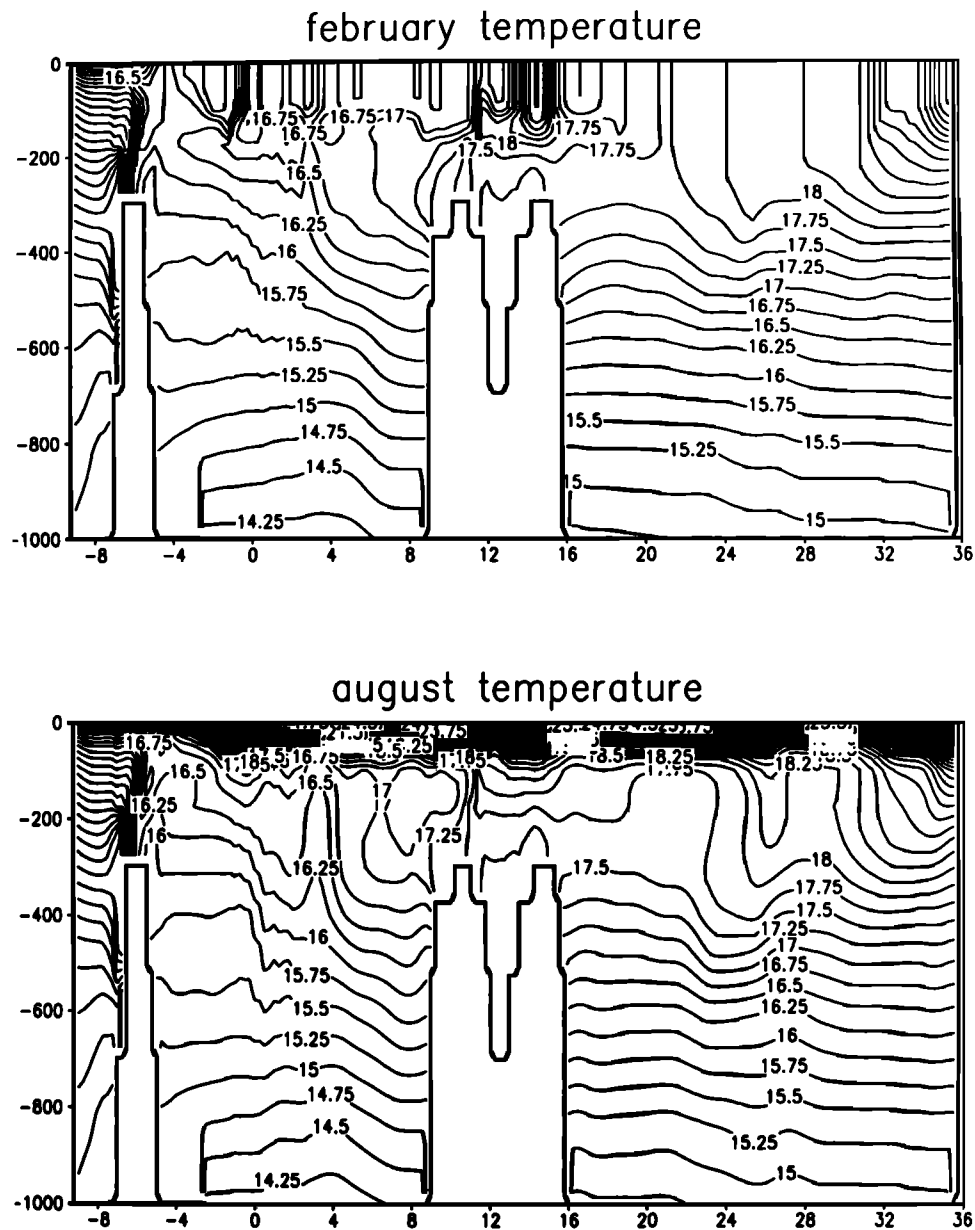


Figure 12a. East-west temperature and salinity sections across the whole extension of the basin (the exact position of the section is indicated above the salinity profiles, in the small rectangle) for February and August (experiment PY2).

the westernmost end of the section, we can recognize the sharp temperature front at Gibraltar which separates the Atlantic 15°C waters from the Mediterranean 16.25°C waters at 250 m of depth. During the winter the Atlantic water (AW) is found at the surface almost everywhere along the section in the western basin, with salinities ranging from 36.5 to 37.5 at the Strait of Sicily. Throughout the year the Strait of Sicily is the site of strong subsurface frontal structures both in temperature and salinity. During summer a steep seasonal thermocline is formed, and we can see the surface salinities increasing eastward. However, a subsurface minimum in salinity is found at ~28°E on the eastern flank of the Rhodes Gyre. This indicates that in some positions the model tries to produce the summer AW subsurface minimum. On the other hand, this process seems relatively easy to produce, as it has already been simulated by the more idealized models of

Pinardi and Navarra [1993]. Thus we conclude that this subsurface salinity minimum is mainly due to advective and mixing processes. This section of Figure 12a cuts through the Rhodes Gyre, which is evident during both winter and summer by the upward sloping of the isotherms at about 400 m of depth and about 27°E. During summer a “patch” of LIW occupies the western flank of Rhodes Gyre, defined by the subsurface salinity maximum shown in Figure 12a at ~25°E. The mixed layer depth at the top of the Rhodes Gyre is the deepest part of the basin, reaching 250 m. Thus LIW is formed in the model each winter, although at shallower depths than actually occur, owing to the warmer temperatures. The subsurface Rhodes Gyre signature seems to be too deep, probably as a result of the “climate drift” of the model which slowly erodes the main thermocline. We can in fact expect that in $T = 70$ years (the length of the integra-

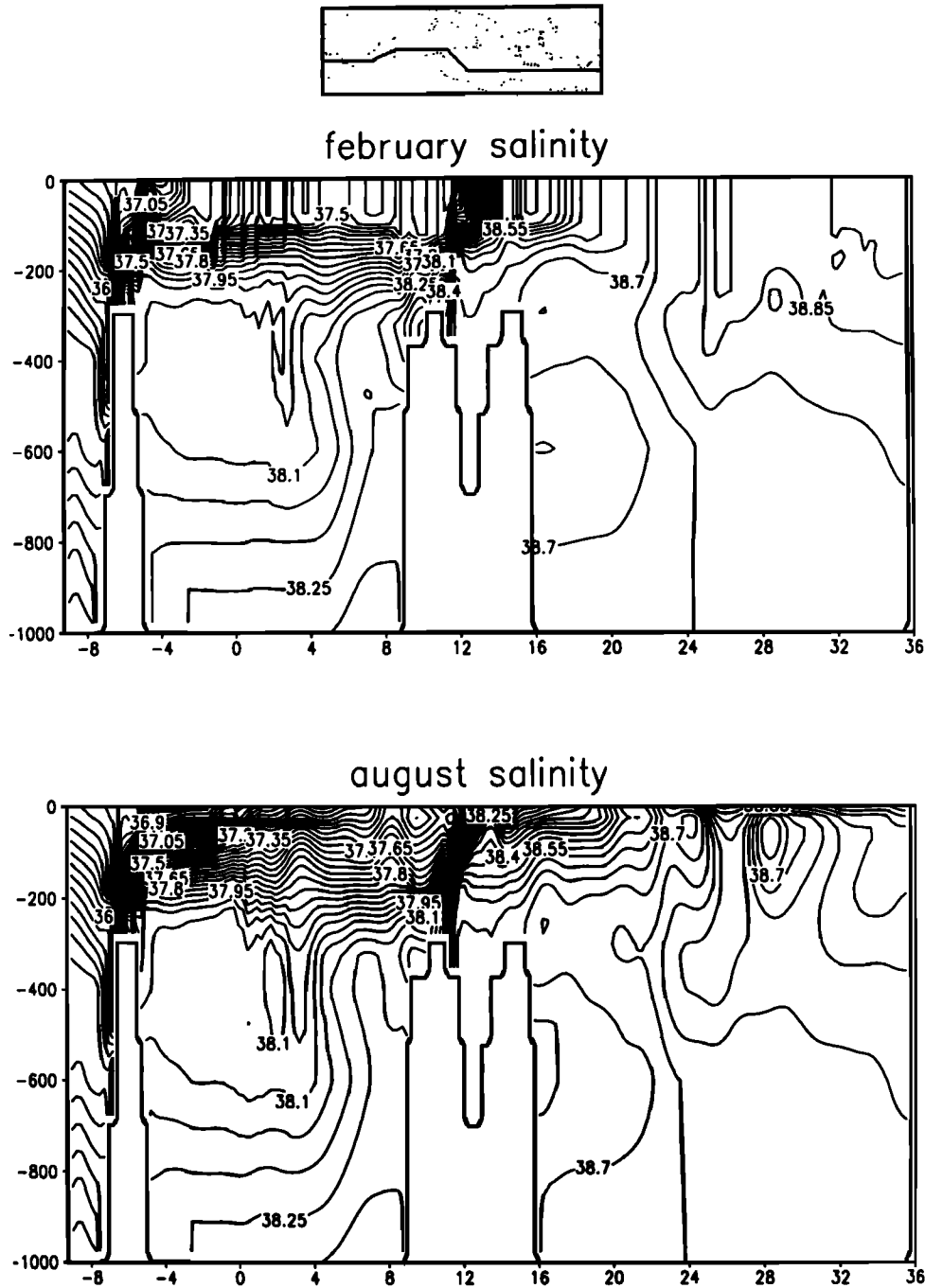


Figure 12a. (continued)

tion), heat would be mixed down from the surface to about 500 m because $H = (K_v T)^{1/2} \approx 450$ m, where K_v is the vertical diffusivity in the model. The thermocline gradients at 200–300 m would be decreased and carried over to deeper regions. The air-sea fluxes which we impose at the interface have a bias which would produce a yearly heat gain in the ocean. As a result of this, the ocean tries to warm up and to correct for this trend; we should use higher-frequency atmospheric forcing, clouds, and “tuned” air-sea interaction (correct albedo and stability dependent coefficients for latent and sensible heat fluxes). This is discussed by Castellari et al. (submitted manuscript, 1995) and is found to correct for a large amount of the climate drift of the model.

A section across the Lyon Gyre is shown in Figure 12b. The sharp upward slope of the isotherms during both summer and winter shows the subsurface structure of the gyre. The seasonal cycle shows capping of the dome during summer by a sharp temperature gradient and during the winter the formation of a mixed layer 250–350 m deep. The salinity mixed layer is deeper than the respective temperature layer. This convective mixed layer is not deep enough to renew the deep waters of the basin. Thus we conclude that we do not produce deep waters, probably due to the rather low heat loss at the sea surface during the winter season (see Figure 3c). The sea surface temperatures are in fact too warm to produce deep waters. It is well known by now that

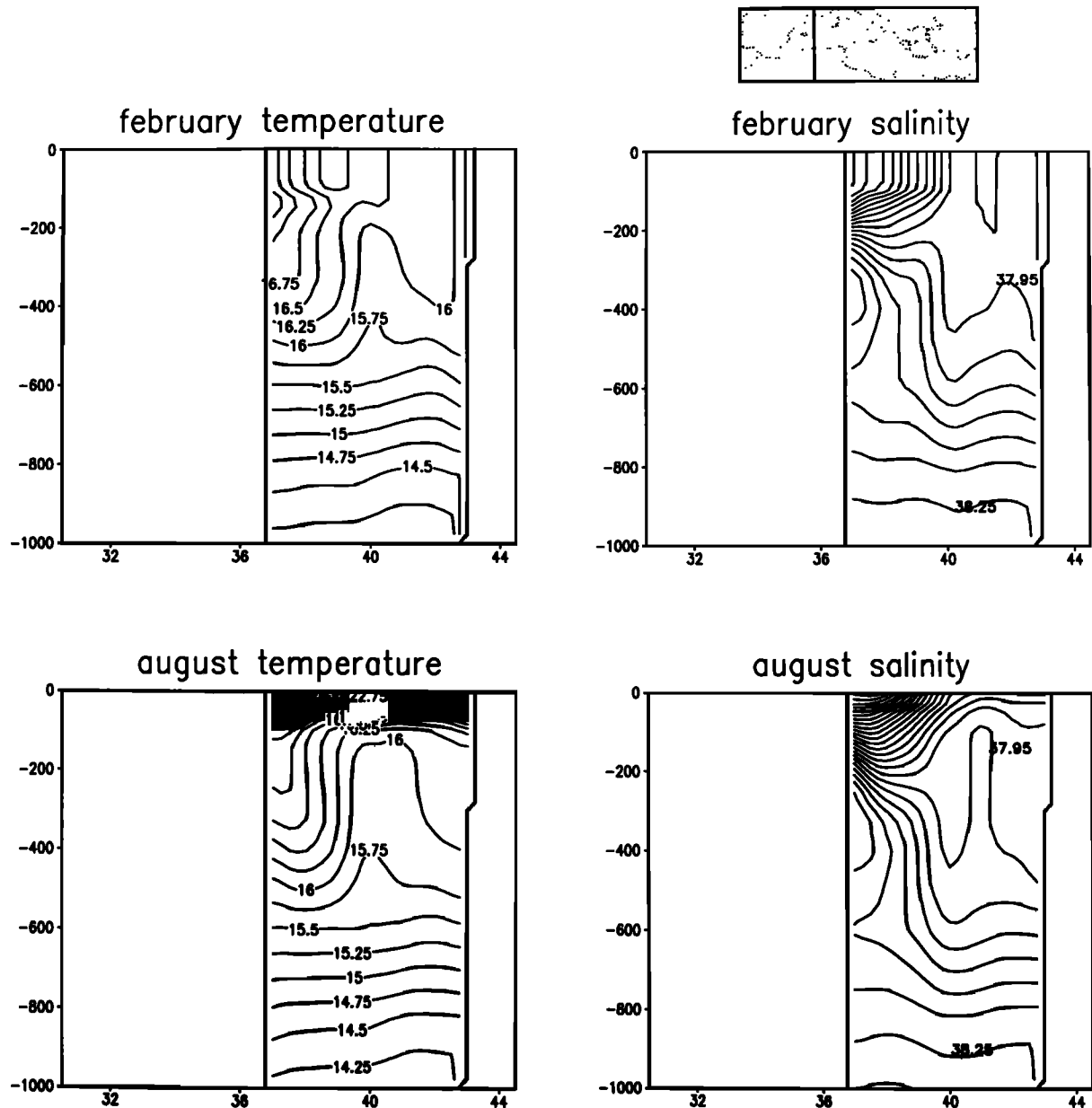


Figure 12b. North-south section of temperature and salinity across the Lyon Gyre (the exact position of the section is indicated in the small rectangle) for February and August.

it is possible to produce deep waters by imposing a priori the correct temperature and salinity at the surface, as shown by Stanev *et al.* [1989]. Our inability to produce this is due to the fact that given the air-sea interaction physics of (14)–(20), the model produces high sea surface temperatures to allow for a small negative Q_u and thus a minimum of Q during winter. In this region, Zavatarelli and Mellor [1995] are also unable to form deep waters. The particular combination of heat fluxes and water column stratification produces a bias in the model. We believe that the open ocean deep water formation processes in this area are the complicated result of heat forcing at the surface, the distribution of temperature and salinity at preconditioning time, and the physical mixing parameterizations represented in the model. At present none of these parameters are adequately reproduced by the GCMs in the area.

In Figure 12c we show a north-south section across the southern Adriatic and the Ionian basin. The sill of Otranto is defined by the bottom rise to about 700 m at $\sim 41^\circ\text{N}$. The center of the Ionian during the winter is occupied by a pool of LIW at about 250 m of depth, partially compensated in density by the corresponding temperature maximum. During the summer this LIW pool shifts to the north and deepens to about 100 m. At the same time, the temperature field forms a subsurface uniform layer in the position of the winter subsurface maximum. The presence of this isothermal subsurface layer was found in the Ionian during one of the POEM cruises [POEM Group, 1992]. It is reproduced here to some degree as a combined effect of the thermal and wind forcing in the basin. We do not produce new deep waters from the Adriatic since the deep isotherms and isohalines at the location of the Otranto sill are unchanged in the course of

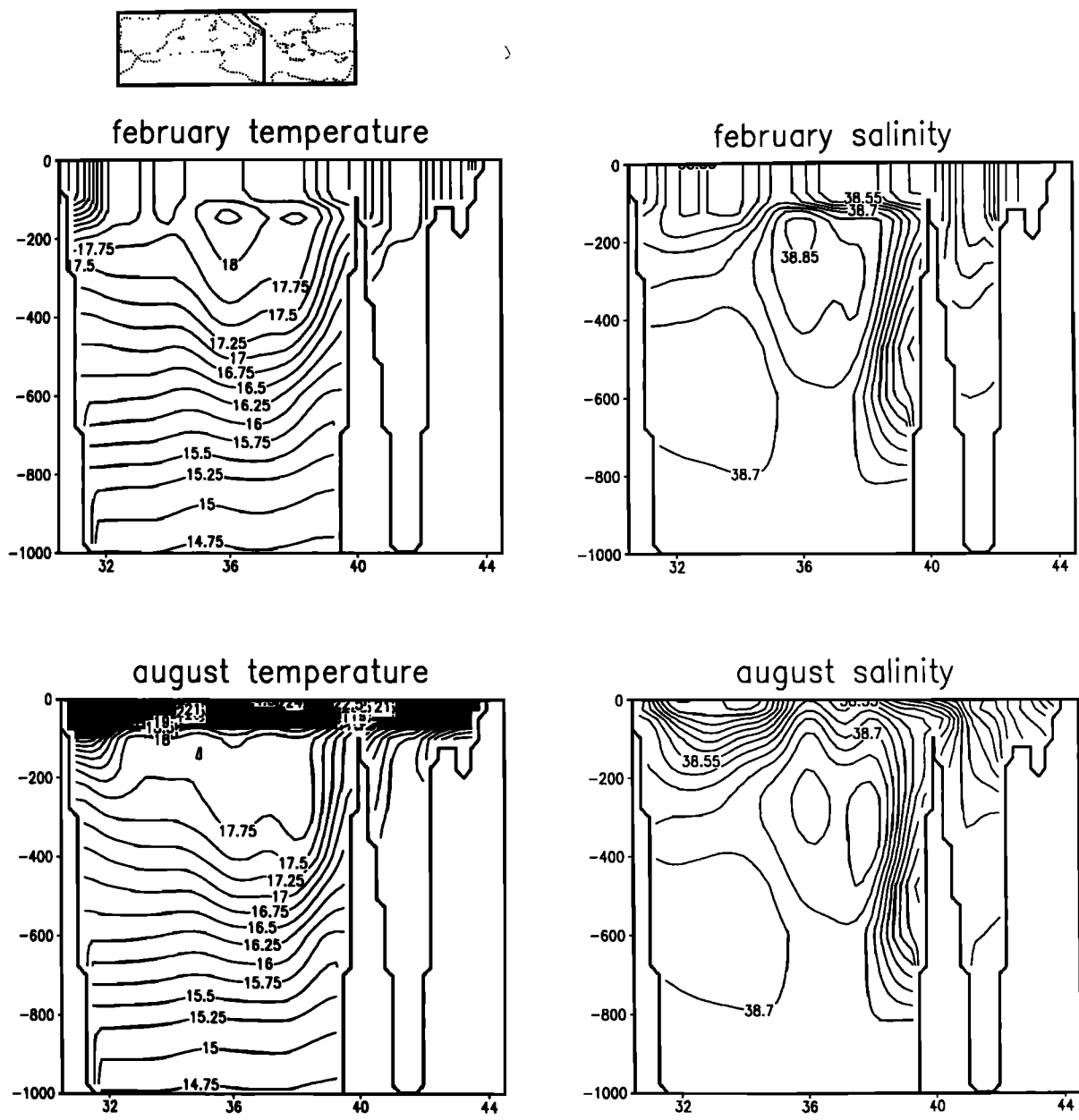


Figure 12c. Same as Figure 12b but for a section across the southern Adriatic and the Ionian basin.

the integration. On the other hand, *Zavatarelli and Mellor [1995]* seem to show deep water renewal from the southern Adriatic. Again, we argue that this is due not to any intrinsic inability of the model to convect water in depth but to the warm bias of the model, which produces higher temperatures than the one present below 1000 m. In PY2 in fact, the southern Adriatic is very well mixed during winter, showing the effects of deep convective mixing, but the temperatures are 3° higher than required for the waters to slide down to the bottom of the Ionian.

3.4. Sensitivity to External Forcings

In Table 1 we present four sensitivity experiments done with different atmospheric forcing fields and Gibraltar open

or closed. In particular, we contrasted the results obtained with HR winds and restoring temperature and salinity boundary conditions to NMC forcing with or without complete heat fluxes.

The NMC and HR experiments of Table 1 are similar among themselves but very different from PY1. The most important difference is the absence of the Mersa-Matruh Gyre in HR and NMC. Thus we conclude that the Mersa-Matruh is due to the seasonal variability in our surface heat fluxes. *Zavatarelli and Mellor [1995]* and *Malanotte-Rizzoli and Bergamasco [1991]* relate their inability to produce such a gyre to the use of *May [1982]* heat fluxes, which are not adequate. We seem to have overcome this problem probably because of the particular forcing data set which we used.

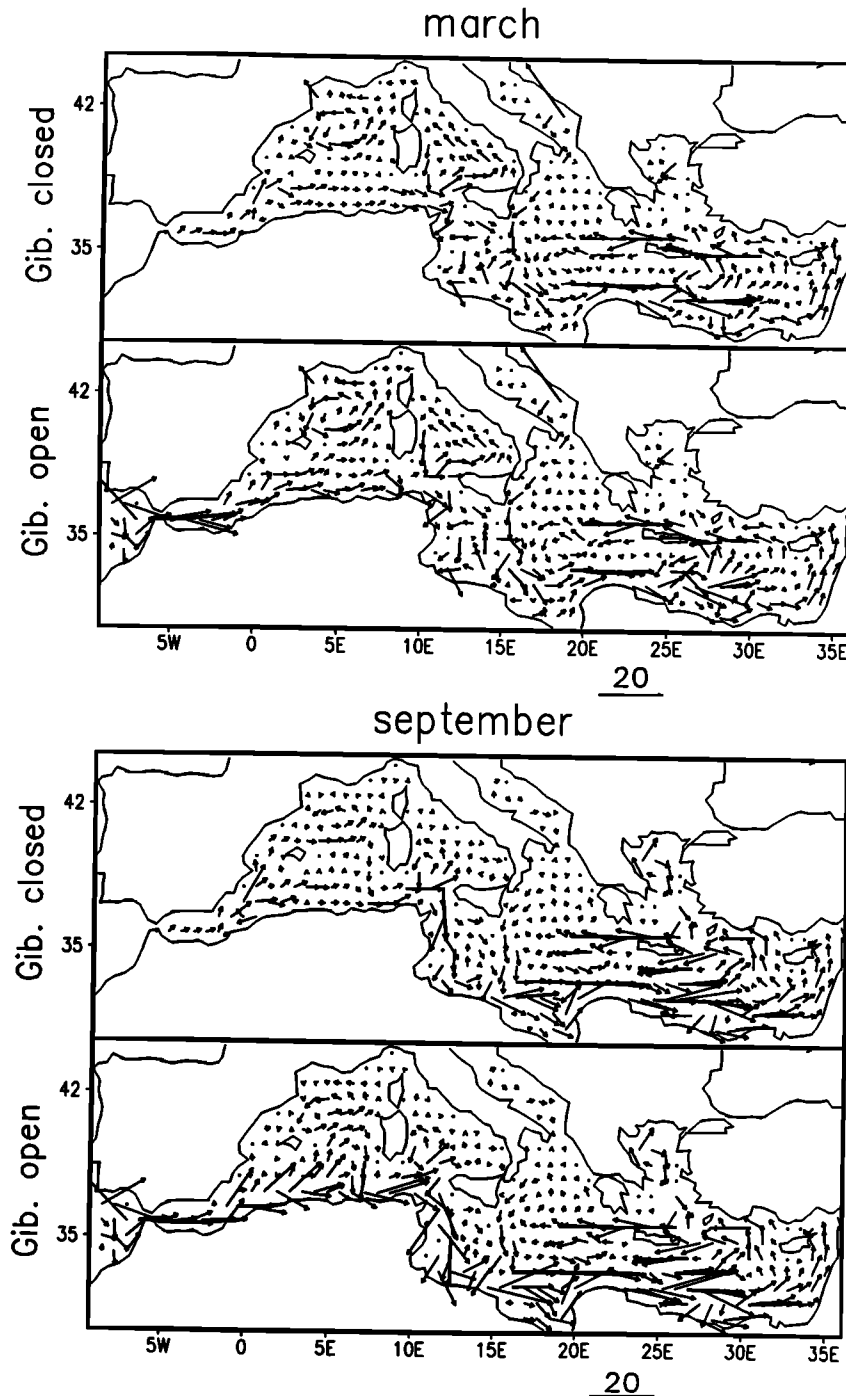


Figure 13. Comparison of baroclinic velocity vector at 30 m for GC and PY1 experiments (see Table 1) and (top) March and (bottom) September conditions. The reference arrow is also indicated.

Another difference between HR and NMC experiments is in the intensity of the Lyon Gyre, which is larger in the HR experiment due to the stronger mistral wind stresses.

The most interesting results are shown, however, by comparing the GC and PY1 experiments. In Figure 13 we show a comparison between the baroclinic velocity field in the GC experiment and PY1 for March and September. The comparison shows that the Algerian current system is very different. In fact, we note that the increased meandering of the Algerian current during summer is totally absent in the GC experiment.

Relevant differences are present in the Ionian and Rhodes Gyre regions where the intensity of the jets and local gyres is very different in the two cases. The split of the Ionian Atlantic stream in the Ionian basin is marked only in the PY1 experiment. In the same experiment the Rhodes Gyre area is more concentrated in the western part of the Levantine basin. It is interesting to note that in the Ligurian Sea (between the northern tip of Corsica and the Italian-French coastlines), there is a well-defined current in summer in PY1 but not in GC. This is an important current system of the WM which has been speculated in the past [Astraldi *et al.*,

1990] to be connected to the overall basin vorticity balance. Here we show that it is definitely connected to the presence of the Gibraltar inflow-outflow system, in agreement with previous results of *Pinardi et al.* [1985].

4. Conclusions

We conclude by summarizing the seasonal characteristics of the Mediterranean general circulation evidenced by the PY2 experiment. We summarize first the WM and EM circulation separately.

Western Mediterranean. The general circulation is composed of two major cyclonic gyres in the northern Provençal-Algerian and Tyrrhenian basins and a surface Algerian current. The Lyon Gyre is a persistent feature of the circulation, and it is coherent with depth. The surface Tyrrhenian Gyre shrinks and propagates westward during summer, and in the eastern part of the basin an anticyclonic gyre forms. This summer anticyclonic gyre in the Tyrrhenian is an example of a seasonally recurrent gyre. We find evidence for this reversal also in the work by *Zavatarelli and Mellor* [1995] and good agreement with the TMR summer flow field. Also, *Heburn* [1987] shows the same features and seasonal variabilities. The LIW path from the Strait of Sicily branches into three parts, one going into the Tyrrhenian, the second along the Sardinia western coastline, and the third along the Algerian-Moroccan coastlines. The seasonal variability of this current system is large, especially at 300 m. The deep waters are not renewed in the WM even though a deep winter mixed layer is produced in the Lyon Gyre and only intermediate waters are formed during winter.

Eastern Mediterranean. Two major cyclonic centers are found to be persistent throughout the year. The first is a western Ionian cyclonic gyre, and the second the well-known Rhodes Gyre. The Ionian stream and the mid-Mediterranean jet are produced by the model simulation at the approximate location given by the observational evidence. For the first time a Mersa-Matruh Gyre is produced by a seasonal integration of a GCM. This feature is shown to have a large seasonal cycle in strength, reaching maximum amplitude during summer. Furthermore, we show that the Mersa-Matruh Gyre is essentially due to our representation of the heat flux forcing at the air-sea interface. The barotropic and baroclinic circulation shows seasonally recurrent gyres in the northern Ionian and the southern Levantine basin. Generally, the southern Levantine anticyclonic motion reaches maximum amplitude during the summer.

Overall we produce a realistic summer warming of the surface layers and subsequent winter mixing of the first 100–150 m of the water column. In fact, the LIW formation process occurs at relatively shallow depths; for example, the LIW formed is too light and it is not convected deeper than 250 m. The deep waters are not formed because of the climatological weak cooling generated by the model surface fluxes. Minimum values of approximately -150 W/m^2 are achieved during winter, while the measurements indicate in the same area approximately -500 W/m^2 of heat loss [*Leaman and Schott*, 1991].

It is our understanding that some of the simulated structures of the general circulation of the Mediterranean basin agree with the observational evidence of the seasonal cycle of the basin, except perhaps below the main thermocline, where we seem to produce more variability than in TMR. It

is true, however, that the observations are poor below 400–500 m and that the measurements are more representative of summer than winter conditions, due to data scarcity in the latter season. Our experiments have offered the opportunity of discussing a possible structure of the seasonal variability of the Mediterranean general circulation. The problem of the realistic representation of the seasonal structure of the general circulation of the basin is still largely unresolved from both the observational and the numerical modeling point of view. The considerable differences between the climatological forcing data sets and the sensitivity of the ocean response to these different forcings suggest the need for using higher temporal resolution atmospheric data sets which take into account the synoptic and interannual fluctuations.

At this stage we can perhaps start to unravel some of the discrepancies between the different observational pictures of the basin general circulation (compare, for example, *Lacombe and Tchernia* [1975] and *Ovchinnikov and Fedoseyev* [1965] with *Robinson et al.* [1991]). The seasonal variability of the basin and perhaps the interannual components of the flow field make the definition of the basin general circulation, on the basis of sparse data sets, extremely difficult and controversial.

Acknowledgments. This work was partially supported by the EC contract "Mermaids" (MAST-CT90-0039) and Mermaids-II (MAS2-CT93-0055). Partial support also came from Mecca project 93311007 for supercomputer time at NCAR. We would like to thank W. R. Holland and A. Navarra for the stimulating discussions during the duration of the research. G. Korres helped to prepare some of the pictures, and the discussions with the overall Mermaids group were invaluable to the work.

References

- Artale, V., M. Astraldi, G. Buffoni, and G. P. Gasparini, Seasonal variability of gyre-scale circulation in the northern Tyrrhenian Sea, *J. Geophys. Res.*, **99**, 14,127–14,137, 1994.
- Astraldi, M., G. P. Gasparini, and G. M. R. Manzella, Temporal variability of currents in the eastern Ligurian Sea, *J. Geophys. Res.*, **95**, 1515–1522, 1990.
- Beckers, J.-M., Application of a 3D model to the western Mediterranean, *J. Mar. Syst.*, **1**, 315–332, 1991.
- Bryan, K., A numerical model for the study of the world ocean, *J. Comput. Phys.*, **4**, 347–376, 1969.
- Bryan, F. O., and W. R. Holland, A high resolution simulation of the wind and thermohaline driven circulation in the North Atlantic Ocean, in *Parametrizations of Small-Scale Processes, Proceedings of the Hawaiian Winter Workshop*, special publication, edited by P. Muller and D. Henderson, Hawaii Inst. of Geophys., Univ. of Hawaii at Manoa, 1989.
- Bryden, H. L., E. C. Brady, and R. D. Pillsbury, Flow through the Strait of Gibraltar, in *Seminario Sobre la Oceanografía Física del Extremo de Gibraltar*, edited by J. L. Almazan, H. Bryden, T. Kinder, and G. Parrilla, Secege, Madrid, 1988.
- Castellari, S., and N. Pinardi, A new perpetual year model of the Mediterranean circulation, *Tech. Rep.*, **1-94**, Ist. per lo Stud. delle Meted. Geofis. Ambient., Modena, Italy, 1994.
- Cox, M. D., An eddy resolving numerical model of the ventilated thermocline, *J. Phys. Oceanogr.*, **15**, 1312–1324, 1985.
- Heburn, G. W., The dynamics of the western Mediterranean Sea: A wind forced case study, *Ann. Geophys.*, **5B**(1), 61–74, 1987.
- Heburn, G. W., The dynamics of the seasonal variability of the western Mediterranean circulation, in *Seasonal and Interannual Variability of the Western Mediterranean Sea, Coastal Estuarine Stud.*, vol. 46, edited by P. E. La Violette, pp. 249–285, AGU, Washington, D. C., 1994.
- Hellerman, S., and M. Rosenstein, Normal monthly wind stress

- over the world ocean with error estimates, *J. Phys. Oceanogr.*, **17**, 158–163, 1983.
- Jones, H., and J. Marshall, Convection with rotation in a neutral ocean: A study of open ocean deep convection, *J. Phys. Oceanogr.*, **23**, 1009–1039, 1993.
- Lacombe, H., and P. Tchernia, Caractères hydrologiques et circulation des eaux en Méditerranée aperçus sur l'apport à l'oceanographie physique des recherches recentes en Méditerranée, *Newsl. Coop. Invest. Mediter., Spec. Issue*, **7**, 25 pp., 1975.
- Lascaratos, A., R. G. Williams, and E. Tragou, A mixed-layer study of the formation of Levantine intermediate water, *J. Geophys. Res.*, **98**, 14,739–14,749, 1993.
- Leaman, K. D., and F. A. Schott, Hydrographic structure of the convective regime in the Gulf of Lyons: Winter 1987, *J. Phys. Oceanogr.*, **21**, 573–596, 1991.
- Levitus, S., Climatological atlas of the world ocean, *NOAA Prof. Pap.* **13**, 173 pp., U.S. Govt. Print. Off., Washington, D. C., 1982.
- Lowe, P. R., An approximating polynomial for the computation of the saturation vapor pressure, *J. Appl. Meteorol.*, **16**, 100–103, 1977.
- Madec, G., M. Chartier, P. Delecluse, and M. Crepon, A three-dimensional study of deep water formation in the northwestern Mediterranean Sea, *J. Phys. Oceanogr.*, **21**, 1349–1371, 1991.
- Malanotte-Rizzoli, P., and A. Bergamasco, The circulation of the eastern Mediterranean, I, *Oceanol. Acta*, **12**(4), 335–351, 1989.
- Malanotte-Rizzoli, P., and A. Bergamasco, The wind and thermally driven circulation of the eastern Mediterranean Sea, II, The baroclinic case, *Dyn. Atmos. Oceans*, **15**, 355–371, 1991.
- May, P. W., Climatological flux estimates in the Mediterranean Sea, *NORDA Rep.* **54**, 57 pp., Nav. Oceanogr. and Atmos. Res. Lab., Stennis Space Center, Miss., 1982.
- Miller, A. R., The Mediterranean Sea, A, Physical aspects, in *Estuaries and Enclosed Seas*, edited by B. H. Ketchum, pp. 219–238, Elsevier, New York, 1983.
- Millot, C., Mesoscale and seasonal variabilities of the circulation in the western Mediterranean, *Dyn. Atmos. Oceans*, **15**, 179–214, 1991.
- Ovchinnikov, I. M., On the water balance of the Mediterranean Sea, *Oceanology*, Engl. Transl., **14**, 198–202, 1974.
- Ovchinnikov, I. M., and A. F. Fedoseyev, The horizontal circulation of the water of the Mediterranean Sea during the summer and winter seasons, in *Basic Features of the Geological Structure, Hydrological Regime and Biology of the Mediterranean*, edited by L. M. Fomin, translated from Russian by the Institute of Modern Languages, pp. 185–201, Nav. Oceanogr. Off., Stennis Space Center, Miss., 1965.
- Ozsoy, E., U. Unluata, T. Oguz, M. A. Latif, A. Hecht, S. Brenner, J. Bishop, and Z. Rosentraub, A review of the Levantine basin circulation and its variability during 1985–1988, *Dyn. Atmos. Oceans*, **15**, 421–456, 1991.
- Pacanowski, R. C., K. Dixon, and A. Rosati, README file for GFDL-MOM 1.0, Geophys. Fluid Dyn. Lab., Princeton, N. J., 1990.
- Philander, S. G. H., W. J. Hurlin, and A. D. Siegel, Simulation of the seasonal cycle of tropical Pacific Ocean, *J. Phys. Oceanogr.*, **17**, 1986–2002, 1987.
- Pinardi, N., and A. Navarra, Baroclinic wind adjustment processes in the Mediterranean Sea, *Deep Sea Res., Part II*, **40**, 1299–1326, 1993.
- Pinardi, N., A. Trevisan, and A. Speranza, Inertial circulation of the western Mediterranean, *Nuovo Cimento Soc. Ital. Fis. C*, **8**(6), 822–841, 1985.
- Physical Oceanography of the Eastern Mediterranean (POEM) Group, General circulation of the eastern Mediterranean, *Earth Sci. Rev.*, **32**, 285–309, 1992.
- Robinson, A. R., M. Golnaraghi, W. G. Leslie, A. Artegiani, A. Hecht, E. Lazzoni, A. Michelato, E. Sansone, A. Theocharis, and U. Unluata, Structure and variability of the eastern Mediterranean general circulation, *Dyn. Atmos. Oceans*, **15**, 215–240, 1991.
- Roether, W., and R. Schlitzer, Eastern Mediterranean deep water renewal on the basis of chlorofluoromethane and tritium data, *Dyn. Atmos. Oceans*, **15**, 333–354, 1991.
- Rosati, A., and K. Miyakoda, A general circulation model for the upper ocean circulation, *J. Phys. Oceanogr.*, **18**, 1601–1626, 1988.
- Roussenov, V. M., and P. Brasseur, Climatological fields in the western Mediterranean: A comparison between objective analysis and variational inverse methods, progress report, Univ. of Liege, Liege, Belg., 1991.
- Stanev, E. V., H. J. Friedrich, and S. V. Botev, On the seasonal response of intermediate and deep water to surface forcing in the Mediterranean Sea, *Oceanol. Acta*, **12**(2), 141–149, 1989.
- Tzipermann, E., and P. Malanotte-Rizzoli, The climatological seasonal circulation of the Mediterranean Sea, *J. Mar. Res.*, **49**, 411–434, 1991.
- Zavatarelli, M., and G. L. Mellor, A numerical study of the Mediterranean Sea circulation, *J. Phys. Oceanogr.*, in press, 1995.

V. Artale, ENEA-CRE, Strada Provinciale Anguillarese 301, 00060 Rome, Italy.

N. Pinardi, IMGA-CNR, Via Emilia Est 770, 41100 Modena, Italy. (e-mail: pinardi@aida.bo.cnr.it)

V. Roussenov and E. Stanev, Department of Meteorology and Geophysics, University of Sofia, 5 Anton Ivanov Boulevard, 1126 Sofia, Bulgaria.

(Received March 12, 1993; revised September 30, 1994; accepted October 5, 1994.)